SYNTHESIS OF GRAPHENE-BASED NANOSTRUCTURED METAL OXIDE SEMICONDUCTORS USING PULSED LASER ABLATION TECHNIQUE

BY

REDHWAN ABDO QASEM MOQBEL

A Thesis Presented to the

DEANSHIP OF GRADUATE STUDIES

KING FAHD UNIVERSITY OF PETROLEUM & MINERALS

DHAHRAN, SAUDI ARABIA

In Partial Fulfillment of the
Requirements for the Degree of

MASTER OF SCIENCE

In

PHYSICS

FEB 2018

KING FAHD UNIVERSITY OF PETROLEUM & MINERALS
DHAHRAN 31261, SAUDI ARABIA

DEANSHIP OF GRADUATE STUDIES

This thesis, written by **REDHWAN ABDO MOQBEL** under the direction of his thesis adviser and approved by his thesis committee, has been presented to and accepted by the Dean of Graduate Studies, in partial fulfillment of the requirements for the degree of **MASTER OF SCIENCE IN PHYSICS**.

Thesis Committee

M. A. Gondal
Dr. Mohammed Gondal (Adviser)

(Co-adviser)

Khalil Ziq
Dr. Khalil A. Ziq (Member)

Dr.Anwar Ul-Hamid (Member)

(Member)

Dr. Abdulaziz H. M. Al-Aswad
Department Chairman

Dr. Salam A. Zummo
Dean of Graduate Studies

28/10/18
Date

عمادة الدراسات العليا
DEANSHIP OF GRADUATE STUDIES

To the soul of my father Allah mercy with him
To my mother
To my brothers
To my wife and Daughter

ACKNOWLEDGMENTS

Praise and glory are due to Almighty Allah (SWT) for his limitless blessings and guidance and may Allah bestow his peace on the prophet, Muhammad (PBUH).

I wholeheartedly acknowledge the assistance offered by King Fahd University of Petroleum and Minerals. I would like to express my deep thanks to Dr. Mohammed Ashraf Gondal, my thesis advisor, for the enormous support he provided me throughout my thesis work. I do not have enough words to express my gratitude for his guidance, support, and motivations. He was my source of inspiration, mentor, and friend at KFUPM. I am also grateful for Dr. Khalil A. Ziq for his support. Also, I offer sincerest gratitude to Dr. Anwar Ul-Hamid for his continuing assistance and constructive comments on my work. I cannot forget my friends at KFUPM, all of them were in a great support to me. Special thanks to my brother, Mohamed Abdo Moqbel for the support and encouragements and to my brother Marwan Abdo Moqbel, Dr.Talal Farhan, Mr. Abdullatif Albaseer, Mr. Hassan Alshab,Mr. Mohamed Yaqot, Mr. Abdullah Alqubalee, Mr. Abu-laise and Mr. Mohammed Hudyan for their help during my thesis work. Acknowledgments are also extended to Dr.Khairee and Mr. Dstageer and Dr. Qasem Darmosh. My ultimate gratitude and love for my parents, sisters, and my wife. Without their

endless support, I would not be able to start and finish my study. I cant thank my parents enough here; may Almighty Allah mercy and forgive my father and give me the opportunity to introduce an ongoing charity to his souls throughout my life. For my wife, you were very supportive and patience especially being away from each other most of the time during my thesis work.

TABLE OF CONTENTS

LIST OF TABLES

LIST OF FIGURES

THESIS ABSTRACT

NAME:	Redhwan Abdo Moqbel
TITLE OF STUDY:	Synthesis of Graphene-based Nanostructured Metal Oxide Semiconductors Using Pulsed Laser Ablation Technique
MAJOR FIELD:	Physics
DATE OF DEGREE:	Feb 2018

This work is associated to the development of a simple and rapid one step synthesis process (where the reaction time is reduced from several hours to a few minutes), which does not require high temperature, toxic chemicals, and any final treatment to remove the unwanted by-products, called pulsed laser ablation in liquids (PLAL) method, for the synthesis of high purity, stable and less agglomeration nanostructured semiconductors. Nanostructured and nanocomposites of CdS, rGO/CdS nanocomposites, ZnO nanostructured and rGO/ZnO nanocomposites were synthesized using PLAL technique. In order to synthesize nanostructured CdS, ZnO, rGO/ZnO and rGO/CdS, we adopted the technique of pulsed laser ablation in liquids (PLAL) to synthesize highly pure CdS NPs and the required CdS/reduced graphene oxide nanocomposites (CdS/rGO) using high pu-

rity (99.9%) microstructured CdS, Zn and GO as chemical precursors. The optical and morphological characterizations revealed that the anchoring of CdS and ZnO on rGO transformed the CdS/rGO and ZnO/RGO composites into an efficient photocatalyst by enhancing the following positive attributes required for a good photocatalyst:

- the inherent tendency of aggregation of CdS and ZnO is considerably reduced, CdS NPs and ZnO NPs with an average grain size of 21 nm are well placed on the rGO sheets, and hence the surface area of the catalyst was significantly increased to provide more active sites.

- The reduced rate of photo induced electron hole recombination manifested in the photoluminescence spectrum indicated the effective charge separation.

- In the visible and infrared region, the photo-catalyst exhibited enhanced absorption, which ensured the effectiveness of this material in naturally abundant solar radiation. In CdS/rGO and ZnO/RGO nanocomposites, the rGO sheets play the role of a supporting matrix, co-catalyst, and electron acceptor for ZnO and CdS. To evaluate the photo-catalytic efficiency of CdS/rGO, we applied it under ,visible irradiation, for degrading methylene blue (MB) dye and found that CdS/rGO nanocomposite was more efficient than bare CdS. Also, to test the photocatalytic activity of ZnO/RGO, we applied it for degrading RhB dye and found that RGO/ZnO nanocomposite was more efficient than bare ZnO under visible irradiation.

ملخص الرسالة

الاسم الكامل: رضوان عبده قاسم مقبل

عنوان الرسالة: تكوين مركبات اشباه الموصلات النانوية مع الجرافين باستخدام الليزر

التخصص: فيزياء

تاريخ الدرجة العلمية: 2018

يرتبط هذا العمل بعملية تسمى , تفتيت المواد الموجودة داخل السوائل باستخدام الليزر, لتكوين مواد نانوية, وهي عملية بسيطة وسريعة حيث تقلل وقت التكوين من عدة ساعات الى بضعة دقائق , علاوة على ذلك هذه العملية لا تحتاج تسخين الى درجة حرارة عالية ولا الى مواد كيميائية سامة , كذلك الا تحتاج الى تنقية الشوائب فالمواد النانوية المنتجة عالية النقاوة واكثر استقرارا. بهذه الطريقة تم تكوين كبريتيد الكادميوم ذي البنية النانوية , والمركب ذي البنية النانوية (كبريتيد الكادميوم مع الجرافين), و اكسيد الزنك ذي البنية النانوية , وكذلك المركب النانوي (اكسيد الزنك مع الجرافين) . وقد اعتمدنا في تكوين المواد والمركبات النانوية السابقة على كبريتيد الكادميوم ذي البنية التركيبية الكبيرة (مايكرو) وعالي النقاوة (99.99%) وكذلك الزنك عالي النقاوة (99.99%) وكذلك اكسيد الجرافين كمواد اساسية للحصول على المركبات النانوية. اظهرت الدراسات للخصائص البصرية والسطحية للمواد والمركبات النانوية بأن المركبات النانوية اصبحت اكثر كفاءة من المواد النانوية وذلك يرجع للاسباب التالية: (1) زيادة السطح المعرض للضوء عن طريق التخفيف من تجمع المواد النانوية حيث توزعت على سطح الجرافين وبالتالي زيادة امتصاص الضوء (2) التقليل من عملية اعادة الاتحاد بين الالكترونات السالبة والفجوات الموجبة وبالتالي زيادة كفاءة المركبات النانوية (3) زيادة امتصاص الضوء في منطقة الضوء المرئي وهذا ادى ايضا الى زيادة فعالية وكفاءة المركبات النانوية مقارنة بالمواد النانوية بدون جرافين. في المركبات النانوية كبريتيد الكادميوم مع الجرافين وكذلك اكسيد الزنك مع الجرافين لعبت اوراق الجرافين دورا هاما في تحسين كفاءة اشباه الموصلات مع كبريتيد الكادميوم وكذلك اكسيد الزنك حيث عملت على زيادة سطح اشباه الموصلات وكذلك لعبت دور اساسي كقابل للالكترونات من اجل التقليل من عملية اعادة لااتحاد بين الالكترونات والفجوات وبالتالي زيادة كفاءة المركبات النانوية. من اجل تقييم كفاءة مركبات اشباه

الموصلات النانوية فقد استخدمنا كبريتيد الكادميوم وكذلك مركب كبريتيد الكادميوم مع الجرافين كحفاز ضوئي لمعالجة وتنقية المياة المحتوية على الصبغة الكيميائية الميثلين الازرق وكذلك اكسيد الزنك و مركب اكسيد الزنك مع الجرافين استخدما كحفاز ضوئي لمعالجة وتنقية المياة المحتوية على صبغة الميثلين البرتقالية وكانت كفاءة المركبات النانوية اكثر من المواد النانوية النقية في تنقية المياه من الاصباغ السابقة الذكر تحت تاثير الضوء المرئي.

CHAPTER 1

INTRODUCTION

Environmental remediation and the quest for reliable alternate energy sources are the two broad, yet interconnected research areas that have direct implication on the present and future human generations and ever deteriorating ecosystem[1]. The advent of nanotechnology and the consequent proliferation of novel materials with ever improving material characteristics have been effectively applied for the remediation of manmade environmental pollution and the generation of efficient photovoltaic cells, an effective and eco-friendly alternate source of energy[2]. Rapid industrialization commands the need for tremendous amount of energy, which is catered by the innumerable power plants which accounts for nearly 30% of greenhouse gas emission [3] and over and above, these industries discharge tremendous amount of hazardous pollutants into air, water and land. The pollution of precious water bodies not only poses a great threat to the availability of potable water, but also imparts enormous negative impact on human and other living organisms [4] [5].Textile industries and the industries dealing with pigment

and dyes discard carcinogenic and non-biodegradable dyes into water bodies and these pollutants wreak havoc to human wellbeing and deplete level of oxygen available for aquatic organisms [6] [7]. Photocatalysis aims at optimum utilization of solar energy with an efficient semiconducting material. Due to mild experimental conditions, availability non depleting solar energy, non-toxicity, low material cost and high efficiency, the semiconductor photo-catalysis has been recognized as an encouraging remediation technique for removing organic, inorganic, and microbes from polluted water [2]. Ever since, the pioneering works on photo-catalysis, many semiconducting materials (TiO_2, ZnO, Fe_2O_3, CdS, WO_3, Bi_2WO_6 and ZnS) have been explored for environmental remediation in general and water purification in particular[8] [2]. Despite the chemical stability and high photo-catalytic activity of the oxide semiconductor, their application as photo-catalysts has been greatly restricted owing to its rapid rate of inherent electron-hole recombination, and low level of light absorption in the visible solar spectral region [9] [10]. Hence all the research efforts have been focussed on developing semiconducting materials, which inherently inhibit the charge recombination and have a good visible light absorption. As nearly 40% of naturally abundant solar radiation is in the visible region, this photocatalyst can be applied for solar energy harvesting [11][12]. Two composites are synthesized by PLAL as presented in the following sections:

1.1 Reduced Graphene Oxide/ Cadmium Solphede (rGO/CdS) Nanocomposites

The light absorption spectrum of a semiconductor is mainly ascribed to its characteristic band-gap energy. In the situation of CdS, the optimal band gap energy (2.42 eV), which made the energy of visible photon with high absorption coefficient (105 cm-1), and this material rose to prominence in the fields of photo-catalysis and photovoltaic applications [13]. However the second constraint is the rapid charge recombination restrict the use of CdS as an effective semiconducting material in photo-catalysis and solar cell applications and improvement of this attribute still remains to be a big challenge [14]. The nanocomposites of CdS with two or more other functional materials have been tried to reduce the charge recombination by the formation of heterojunctions and thereby improving the composite efficiency of the material [15]. In this context, graphene was also used as a composite partner of CdS by many research groups [16][17][18]. The structure of graphene is planar network of sp2 hybridized carbon atoms, closely-packed in a 2-dimensional (2D) honey comb structure [19] and it is well known for its chemical stability, massive surface area (2600 m^2g^-1), excellent electron mobility and high thermal conductivity (5000 $Wm^{-1}K^{-1}$)[19][20][21] . Various methods of synthesis for CdS/rGO nanocomposite were adopted and applied for many photo-catalytic applications. Peng et al used CdS/rGO nanocomposite, synthesized by one-pot solvothermal process for photo-catalytic hydrogen production. Nan et al[22] adopted microwave-assisted solvothermal method to synthesize

CdS/rGO nanocomposite and applied it under visible radiation for the degradation Rhodamine B. Rajendra et.al[23] produced CdS/rGO nanocomposite through chemical bath deposition for degrading Cr(VI). Murillo et.al[24] investigated the influence of GO reduction on the atomic arrangement and photo-catalytic performance of CdS/rGO hybrid system fabricated through solvothermal method. Lei et.al[25] developed a mixing process using ethylene glycol as solvent to prepare CdS/rGO nanocomposite. Nannan et.al[26] used reflux condensation procedure to synthesize CdS/rGO nanocomposite for photo-catalytic uses. Many studies reported that the optimal weight percent of rGO to optimize the photocatalytic efficiency of CdS/rGO nanocomposite is 5% [27][28][29][30][31]. This is attributed to less active CdS surface area directly exposed to the light to absorb photons they are mostly being absorbed by the rGO itself at higher loadings. Although the CdS/rGO nanocomposite synthesized by various methods were found to be successful for photo-catalytic applications, these methods of synthesis have practical challenges such as the need for laborious multistep process (time consuming), the need for different additives to retain graphene structure, the use of toxic chemicals or high temperature to reduce graphene oxide[1][4][16]. In this work, for the first time, we adopted the simple technique pulsed laser ablation in liquids (PLAL) to synthesize high purity CdS NPs and CdS/rGO nanocomposites with a high purity microstructured CdS (99.9%) and a single layer (<450nm) graphene oxide as starting materials. PLAL is one step-process (it reduces the synthesis time manifold from hours to just a few minutes) and does not involve the use of toxic

precursors, elevated temperatures or further post-synthesis processing to remove by-products. Firstly, PLAL was used to synthesize CdS NPs from high purity microstructured CdS. Secondly, same source of laser with same parameters was used to ablate a series of physical mixtures with 5% of a single layer graphene oxide and the as-prepared CdS NPs to synthesize high purity CdS/rGO-5 weight% of GO in as-prepared CdS NPs. CdS NPs with an average grain size of 20 nm are well placed on the rGO sheets, which play the role of a supporting matrix, co-catalyst, and electron acceptor for CdS. The aggregation of CdS NPs over 50 nm were observed in the exclusion of graphene oxides. The anchoring of CdS on rGO brought about the enhancement of two positive features necessary for photocatalytic applications as compared to pure CdS: (i) the absorption is enhanced in the visible/IR region, ensuring the effectiveness of this material in naturally abundant solar radiation and (ii) the reduced photoluminescence, indicating the effective charge separation. In order to affirm this, we applied these materials as a photocatalyst activated by visible illumination for degrading methylene blue (MB) dye and it was found that CdS/rGO-5% were more efficient than pure CdS in the visible region. Therefore, this method provides a simple and one-step route to synthesize high purity visible-light-driven photocatalysts and solar cell material without any need for noble metal-loading.

1.2 Reduced Graphene Oxide/ Zinc Oxide (rGO/ZnO) Nanocomposites.

ZnO is one of the most commonly used semiconductor photo-catalyst, which has a wide band-gap energy of approximately 3.37 eV, high electron mobility, low cost, and above all it is environmentally friendly [32][33][34]. However, pure ZnO is photo-catalytically active only in the UV spectral region and also suffers a great deal of photo-corrosion, high susceptibility to dissolve at the extreme pH value in aqueous solution under UV [35]. With proper modification, ZnO can be made functional catalyst in the visible spectral region, which accounts for 47% in the solar radiation as compared to 57% of UV content in the solar spectrum and naturally the above mentioned problems of photo corrosion and the solubility issues of ZnO are drastically minimized in the visible region [36][37]. Besides transforming ZnO into visible light active, the modifications on ZnO (doping with other elements, dye sensitization, and formation of composite with other semiconductor materials) have been employed to bring about an important positive feature, namely the reduced electron-hole recombination rate in the photo-catalyst[32][38][39][40][41][42][43]. Yet another problem associated with ZnO as a photo-catalyst is its natural tendency to aggregate into a larger particle and this property is not desired in any photo-catalyst as this leads to the reduction of active surface area and consequent reduction in the active sites for the reactants on the catalytic surface[44]. Graphene-based materials, are commonly used as the composite material in the photo-catalyst to improve the photo-catalytic

efficiency, due to their high thermal stability, massive specific surface area and high conductivity. [45][46][47][48][49]. However, graphene oxide (GO) is preferred to graphene (GR) due to the formers stronger interaction in the hybrid composite through the oxygen containing functional groups, and also in order to further improve the function of the composites, GO sheets are partially reduced to get reduced graphene oxide (rGO), because the conductivity of GO sheets are considerably enhanced in the reduction process [50][51][52]. Several groups have reported the synthesis of ZnO/rGO by different methods such as microwave-assisted reaction, hydrothermal, solvothermal, hydrolysis methods, thermal expansion of GO under inert atmosphere by nitrogen, surface coating and liquid arc discharge [53][54][55][56][57][58][59] with different weight per cent of rGO in ZnO/rGO and it was consistently established that weight ratio of about 4% rGO in ZnO/rGO is the optimum to enhance the photo-catalytic efficiency of this nanocomposite [60][61][62][63]. This optimum weight per cent of rGO in ZnO/rGO exists because this quantity of rGO is sufficient to bring out the positive features expected from its presence and any amount above this level will block the active ZnO sites and instead rGO itself absorb the light, which is not desirable[60].Although ZnO/rGO nanocomposite synthesized by various methods were found to be successful for photo-catalytic applications, these methods of synthesis have practical challenges such as the need for laborious multistep process (time consuming), the need for different additives to retain graphene structure, the use of toxic chemicals or high temperature to reduce graphene oxide[60][64]. In this work, for the first time, the

simple technique of pulsed laser ablation in liquids (PLAL) was used to synthesize high purity ZnO/rGO nanocomposites using microstructured Zn (99.9%) and a single layer (< 450nm) graphene oxide as starting materials. PLAL is a simple and rapid one step-process, which obviates the need for utilising toxic chemicals, elevated temperatures or any further purification process to remove the reaction by-products. The synthesis of ZnO/rGO nanocomposites is carried out in two PLAL processes with same laser and experimental parameters first one to synthesize ZnO NPs from high purity microstructured ZnO, and the second final process to obtain ZnO/rGO nanocomposites, from the mixture of ZnO NPs (obtained from the first PLAL process) and single layer GO (4% weight ratios). The morphological studies on the ZnO/rGO nanocomposites revealed that ZnO NPs with a mean grain size of approximately 30 nm are well placed on the rGO sheets, which play the role of a supporting matrix, co-catalyst, and electron acceptor for ZnO. The presence of rGO sheets reduces the aggregation ZnO NPs and thereby allowing more surface area (more active sites) for the reactants on the catalytic surface. Also the absorption spectra of ZnO/rGO nanocomposites showed that the anchoring of ZnO on rGO sheets enhanced the light absorption in the visible/IR region, which means that the composite material is transformed to be effective in naturally abundant solar radiation. To evaluate the photo-catalytic performance of ZnO/rGO nanocomposites synthesized by PLAL, we carried out a comparative study of this nanocomposites and pure ZnO Nps in the process of photo-catalytic degradation of RhB dye using visible illumination. The results,

as expected showed that the photo-catalytic breakdown performance of RhB dye with ZnO/rGO nanocomposites as a photo-catalyst is considerably more than one with pure ZnO as a photo-catalyst in the visible region. Hence, from this work, it is established that the simple PLAL method can be employed to synthesize high purity visible-light-driven photo-catalysts rather than subjecting the materials for noble metal-loading.

1.3 Objectives

This work aims to synthesize visible-light responsive graphene-based nanostructured semiconductors for water purification using PLAL technique. The particular goals are summarized in the following points: 1- To synthesize nanostructured semiconductor by PLAL

2- To engineer the band gap of nanostructured semiconductors by graphene.

3- To perform characterization studies of the fabricated nanomaterials using different analytical methods.

4- To apply graphene-based nanostructured semiconductors for photo-catalytic water purification.

CHAPTER 2

LITERATURE REVIEW

In this chapter novel published literature is summarized which has attracted great interest for the development of RGO/CdS and RGO/ZnO and using them for removal of pollutants from the water.

2.1 (CdS/RGO) nanocomposites

In 2014,J Wang et al.[65]synthesized CdS/RGO nanocomposites via hydro-thermal method, they spent 16 hours to prepare these nanocomposites. The photo-catalytic efficiency was tested by degradation of RhB under 300 W halogen lamb as a visible light source. They dispersed 0.01 g from CdS/RGO in 20 mL of 1 * $10^{<}-5$ aqueous solution of RhB. When the wight percent of RGO was 3% the degradation efficiency showed the highest value of 91% in 120 min compared with 81% with pure CdS.

In 2014, Hui Liu at al.[66]synthesized CdS/RGO microspheres using hydrothermal method, they spent almost 3 h to prepare the CdS/RGO. The photo-catalytic

activity of the CdS and CdS/RGO microspheres were accomplished using the degradation of RhB under 500W xenon lamb as a visible light source. They dispersed 0.07 g from CdS/RGO in 70 mL of 0.005g/L aqueous solution of RhB. The degradation efficiency showed 95.2% with 50 min compared with 78.1% with pure CdS.

In 2012, Aihua Ye et al.[67]synthesized CdS/graphene (GR) nanocomposites by hydro-thermal method.The photo-catalytic activity was evaluated by degradation of MO under 200 W Xenon arc lamb as a visible light source. They dispersed 0.05 g from CdS/RGO in 50 mL of 0.01 g/L aqueous solution of MO. When the wight percent of RGO was 1% the degradation efficiency showed the highest value of 95% in 60 min compared with almost 20% with pure CdS.

In 2012,Wang et al.[29]fabricated (RGO/CdS) using solvothermal technique. The photo-catalytic efficiency was tested by removal of MB under 300 W Xenon lamb as a visible light source. They dispersed 0.08 g from CdS/RGO in 500 mL of 0.1 g/L aqueous solution of MB. When the wight percent of RGO was 5% the degradation efficiency showed the highest value of 94% in 150 min compared with almost 38% with pure CdS.

In 2013, N Zhang et al.[28]synthesized CdS/RGO nanocomposites using solvothermal approach. The photocatalytic activity was evaluated under a visible light

source by photocatalytic conversion of the toxic heavy metal ions Cr(VI) to Cr(III) in aqueous solution . When the wight percent of RGO was 5%, the degradation efficiency showed the highest value of almost 100% in 20 min compared with almost 39% with pure CdS.

In 2016,Wang et al.[30]synthesized TiO2-CdS/RGO nanocomposites by solvothermal technique. The efficiency was tested using degradation of Methylene blue (MB) dye and Rhodamin B (RhB) dye under 500 W Xenon lamb as a visible light source. They dispersed 0.05 g from TiO2-CdS/RGO in 80 mL of 0.02 g/L aqueous solution of RhB dye and MB dye. When the wight percent of RGO was 5% the degradation efficiency showed the highest value of 97.5% and 93.5% regularly for MB and RhB in 150 min compared with almost 78.5% and 74.8% regularly for MB dye and RhB dye in the case of pure CdS.

In 2014, P Russo et al.[6]synthesized reduced graphene oxide (RGO) using second harmonic of a Nd:YAG pulsed laser with the following parameters: pulse duration = 5 ns and repetition rate = 10 Hz, and they used it for the adsorbents of methylene blue dye (MB).

In 2012,Peng, et al.[12]using facile precipitation technique, the cadmium sulfide (CdS)-graphene oxide (GO) nanocomposites was fabricatedand and Cd(Ac)2,

Na2S, and prefabricated GO were used as raw materials.The nanocomposites was used ,under visible light, for hydrogen production as energy.

In 2016, ME Khan,et al. [16] fabricated (CdS-Graphene) nanocomposite using a simple method. The efficiency of the composites was tested under visible light irradiation by removal of different types of dyes.

In 2017, Priyesh V. et al[68] synthesized a triple hybrid nanocomposite of CdS/RGO/Polyaniline using an in situ prepared technique. The seebeck coefficient was measured for all composites and the CdS/RGO/Polyaniline nanocomposites was the best conductivity.

In 2017, Chakraborty et al. [69] Synthesized CdS/RGO nanocomposites via solvothermal process. The photocatalytic efficiency tested under simulated solar light for removal of 4-Nitrophenol (4-NP). The activity of CdS-RGO composite is 2.6 times more than CdS.

In 2018, Lin, et al[70] fabricated CdS/RGO composites by a facile ultrasonic technique. The Photocatalytic efficiency tested under visible light illumination for the degradation of MB dye. The efficiency of CdS- 10% RGO composites was the best compared with other composites and pure CdS.

In 2018, Singh et al[71] synthesised CdS/RGO using a two steps method from the procourses chemicals. The characterization showed that the CdS/RGO has higher absorption than Pure CdS.

2.2 (ZnO/rGO) nanocomposites

In 2016, J Qin et al.[72] spent more than 16 hours to fabricate (ZnO microspheres RGO) composites using simple method and the efficiency was tested for the degradation of the methylene blue dye (MB) from water using ultraviolet illumination. Different amount of GO was added to ZnO to synthesize ZnO-RGO nanocomposites and the best photocatalytic performance obtained was 4.02% RGO.

In 2015, N Song et al.[61]spent more than 5 hours to synthesis ZnO nanoroads and ZnO-RGO nanocomposites by thermal treatment. Different composites of ZnO-RGO were synthesized with different amount of GO. RGO-ZnO nanocomposites with 4% RGO showed optimal photocurrent and photocatalytic response under UV light.

In 2012, Luo,et al.[62]fabricated (RGO-ZnO) hollow spheres composites via a simple ultrasonic method with different amount of RGO. The photocatalytic efficiency was evaluated ,under ultraviolet light illumination, by the degradation of

MB dye . The RGO-ZnO with 3.56% showed the highest photo-catalytic efficiency under ultraviolet light illumination where for 1.5 hour, nearly all methylene blue dye (MB) was removed using (RGO-ZnO 3.56%) compare with 60% for pure ZnO hollow spheres.

In 2015,Moussa et al.[73]prepared (ZnO rods/RGO) using solvothermal technique. The efficiency of the photo-catalytic was evaluated by removal of orange II dye under 5 mW/cm2 of solar light and 2 mW/cm2 of visible light source. They dispersed 0.06 g from ZnO/RGO in 50 mL of 10 mg/L aqueous solution of Orange II dye. When the wight percent of RGO was 10%, the degradation efficiency showed the highest value of 88% in 150 min.

In 2016,Yao et al. [34]prepared ZnO/RGO nanocomposites via one step sol-gel method. The efficiency of photo-catalytic was tested for RhB removal under visible light. Catalyst 0.08 g was mixed in 5 mL RhB $3 * 10^{-5}$ M aqueous solution and irradiated by 260 W Xe lamb for 20 min as a visible light source. The ZnO-RGO showed better result than pure ZnO where, almost 100% of RhB is decomposed in 16 min but it takes 100 min in the case of ZnO.

In 2017, Ong et al[74] synthesised ZnO/RGO nanocomposites via sol-gel technique. Nanocomposites, under solar light, showed high efficiency for removal of perfluorooctanoic acid and methyl orange, combare with ZnO.

In 2017, Li, et al[75]fabricated ZnO/RGO nanocomposites via hydrothermal method. The characterization show that the properties of nanocomposites is better than ZnO.

CHAPTER 3

EXPERIMENTAL DETAILS

3.1 EXPERIMENTAL METHODS

3.1.1 Preparation of CdS/rGO using PLAL

In PLAL, the second harmonic of a Q-switched Nd-YAG laser (Brilliant B) operating at wavelength of 532 nm was used as a source for laser ablation. This laser operates at the following parameters: maximum energy/pulse = 450 mJ, pulse repetition rate = 10 Hz and pulse width = 5 ns. The laser beam was routed and focused on the sample with an appropriate turning prism and lens.We selected 532 nm as the excitation source, because the absorption of CdS is in the visible region and the photo-generated holes are used to reduce GO to rGO. Initially, the suspension of 100 mg high purity commercially available microstructured CdS (99.9%, Sigma Aldrich) in 20 ml of DI water was made and this solution was irradiated by a focused laser beam (532nm) of energy 280 mJ/ pulse and 0.8 nm beam diameter. To obtain a solution with good homogeneity, a high-speed mag-

netic stirrer was utilized for all parts of this study. After 20 minutes of irradiation, microstructured CdS is transformed into CdS NPs. Subsequently, CdS NPs, synthesized by the above step (by PLAL) were mixed with 5.0% (weight per cent) of a single layer GO ($<$ 450nm, Cheap Tubes) suspension and further subjected to the laser irradiation for about 15 minutes with the same laser parameters. During this process GO gets reduced and becomes rGO and simultaneously the nanostructured CdS NPs anchor on the rGO sheets to form CdS/rGO nanocomposite. 3.1

3.1.2 Preparation of ZnO/rGO using PLAL

An intense pulsed UV laser beam of wavelength 355 nm (third harmonic of Q-switched Nd-YAG laser Brilliant B), 10 Hz pulse repetition rate, 8 ns pulse width and 130 mJ pulse energy was used as a radiation source and this laser beam was directed to the PLAL reaction chamber using appropriate turning prism and lens. The dispersion of high purity commercially available microstructured Zn (99.9%, Sigma Aldrich) in 20 ml of DI water was irradiated by the focused laser beam and the homogeneity of the solution is maintained by keeping the PLAL reaction chamber on the magnetic stirrer. After 40 minutes of irradiation, microstructured Zn transformed into ZnO NPs. For the synthesised of ZnO/rGO nanocomposite, the synthesized ZnO NPs was then mixed with (4.0weight%) of a single layer graphene oxide (<450nm, Cheap Tubes) dispersion and further subjected to the laser irradiation for about 15 minutes. During this process GO gets reduced and

becomes rGO and simultaneously the nanostructured ZnO NPs anchor on the rGO sheets to form ZnO/rGO nanocomposite.The diagrammatic of the synthesis procedure is showed in Figure 3.1

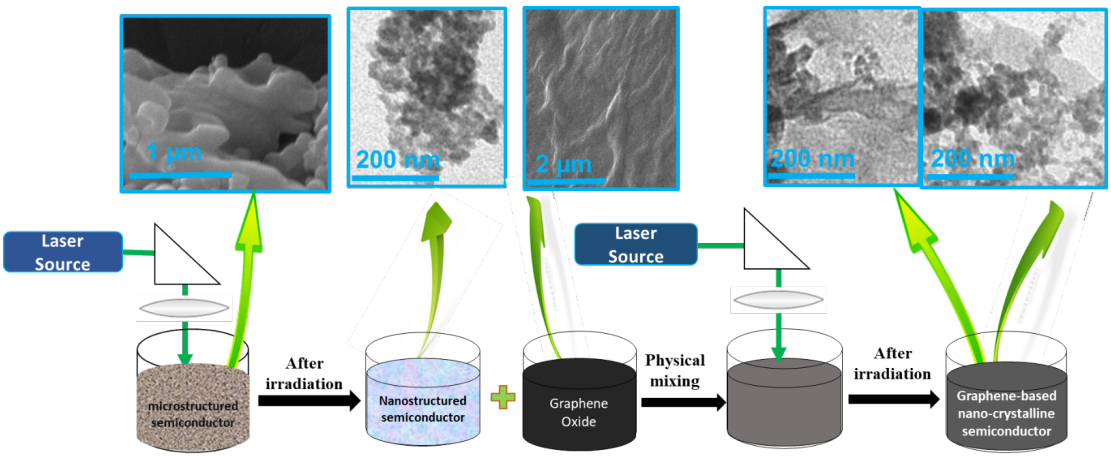

Figure 3.1: The schematic diagram for the synthesis of, CdS-NP, ZnO-NP, rGO-CdS and RGO/ZnO by PLAL method

3.1.3 Material Characterizations

For the XRD studies, XRD, Shimadzu XRD-6000, equipped with a monochromatic wavelength of Cu $K_\alpha X$ ray at 0.15418 nm, operating at 40kV and 40 mA was used. TEM images were obtained using FEI Titan 80-300 CT TEM. For the X-ray photoelectron spectroscopy, ESCALAB-250Xi, Thermos-Scientific with a monochromatic Al K_α (1486.6 eV) was used. Carbon 1s with binding energy of 284.8eV was used as reference for XPS characterization. The defused reflectance spectra (DRS) were taken using ultraviolet-visible spectrometer (JASCO V-670) and for the PL studies Shimadzu spectrofluorometer (RF 5301 PC) with the excitation wavelength of 325 nm was used.

X-ray Diffraction (XRD)

XRD is a nondestructive materials characterization tool employed to identify crystalline phase that maybe present in a material. it also determines structural properties such as; defect structures, epitaxy, grain size, phase composition and preferred orientation.

X-Ray Photoelectron spectroscopy (XPS)

XPS is a tool to analysize the structure of atoms and get information about electron structure as well as ionization energies. Typically, a sample is irradiated with an incident x-ray beam, followed by measuring the energies and numbers of electrons ejected from the sample surface. With this technique we are able to obtain the chemical composition of various materials. It reveals which chemical elements

are present at the surface such as carbon and oxygen, and it informs us about the chemical bound nature which exist between these elements. Xps has some advantages and disadvantages. The first advantage is that it is a non-destructive and highly-surface-sensitive method so is very helpful to elemental mapping, for example. Another advantage is it provides us with quantitative measurements and it gives us information about chemical bounding and the chemical composition of the molecule. On the other hand, it has some disadvantages as well; it is first of all very expensive technique, secondly it needs high vacuum and it is slow process so it might need a whole night to provide results and finally, it detects elements having an atomic number greater than or equals to 3, thus excluding hydrogen and helium.

Uv-Vis spectrophotometry

A special tool which measures the amount of light a substance absorbs. All substances have different transmittance and absorbance coefficient, in much the same way that fingerprints can be used to uniquely identify individual humans. Hence by obtaining the absorption spectrum as a function of wavelength we are able to uniquely identify the substance and composition of different materials. In addition, by detecting the light intensity, Uv-Vis spectrophotometry can quantify the solute concentration present in a sample, also it used to determine the band gap of semiconductor.

Transmission Electron Microscope (TEM)

Transmission Electron Microscope uses a beam of electron instead of light, exploiting the wave-particle duality of electrons. It consists of an electron emission source, electromagnetic lenses and an electron detector. A very thin sample is positioned along the electron beam. The electron beam is produced, accelerated and then focused on the sample by the lenses. The beam passes through the sample which modifies and imprint its image. The beam is then magnified by other lenses and detected, for example using fluorescence.Transmission Electron Microscope (TEM) magnifies images of very thin samples down to atomic resolution. One type of transmission microscopes is the Scanning Transmission Electron Microscope (STEM). Here, the electron beam is concentrated on a specific point of the sample, not on the whole surface. The transmitted beam is then detected. A scanning of the surface allows to visualize here again the magnified images of the sample. In addition, one can measure the transmitted beam characteristics at different locations of the sample. For example, one can measure the electron energy loss(EELS). To do so, a magnetic prism is used to deflect the beam more or less depending on its energy. The more the beam loses energy, the more it is deflected. The measure of this deflation allows to characterize different parts of the samples. This technique allows for example to visualize and also identify the chemical nature of atoms in ultra-thin samples.

3.1.4 Cds/rGO Photo-catalytic Studies

The photo-catalytic activity of CdS NP and Cds/rGO were evaluated by studying their effectiveness in the process of photocatalytic degradation of MB dye under the broad band visible radiation from 300 W Xenon lamp with UV cut-off filter (<390 nm). The intensity of the visible light used for this photo-catalytic degradation is 100 mW/cm2. For this study, 50 mL of 10 mg L1 MB in aqueous solution was mixed with a measure of 80 milligrams of photo-catalyst and these suspensions were subjected to vigorous stirring, using a magnetic stirrer in the dark room for about 30 minutes for establishing equilibrium of the adsorption and desorption of dye on the surface of the photo-catalyst. After this stirring, the photo-catalytic reaction was began by turning on the light radiation source and continuing the stirring till the end of the experiment. 2 ml of the irradiated samples were collected at a regular interval, suspended photo-catalyst were removed with cellulose filter (200 nm) and the absorption spectra were taken using the spectrophotometer to estimate the concentrations of the degraded sample after radiation. The figure of merit used in this study is the percentage of the ratios of degraded dye concentration (C) and the initial dye concentration (C_0), using the intensities of the maximum absorption band at 664 nm. Prior to the actual photo-degradation process, we verified non photocatalytic removal of MB dye by using photo-catalyst in the absence of light (by adsorption of dye on the catalytic surface) and with light in the absence of catalyst (photolysis) and found that the removal of MB dye in the absence of catalyst or light was negligible

3.1.5 ZnO/rGO Photo-catalytic Degradation Studies

Collimated Xenon lamp of 100 W lamp power with a UV cut-off filter (<390 nm) was used as radiation source for the photo-catalytic degradation studies. The experimental sample was 15 ml of RhB dye solution (10 mg/L concentration and the photo-catalyst used for the degradation process was in the form of film, where 3 mL of the catalytic solution (5mg/ mL concentration) was sprayed and dried on the glass substrate of 1 square inch area, fig 3.1 shows degradation experiment setup. The RhB solution with catalytic film was stirred for 30 minutes to accomplish absorptiondesorption balance of the dye on the surface of the photo-catalyst. During the irradiation process, 1.5 ml of sample was collected at a regular interval and the absorption spectra were taken using the spectrophotometer to estimate the concentrations of the degraded samples and the analysed dye sample was returned to the photo-catalytic chamber. The figure of merit used in this study is the percentage of degradation (which is $[(C_0\text{-C})/C_0]$ x 100), where C_0 and C are the initial and instantaneous dye concentrations respectively. The intensity of the absorption peak of RhB centered at 554 nm was used to quantify the concentration of the dye in the aqueous solution.

10.png

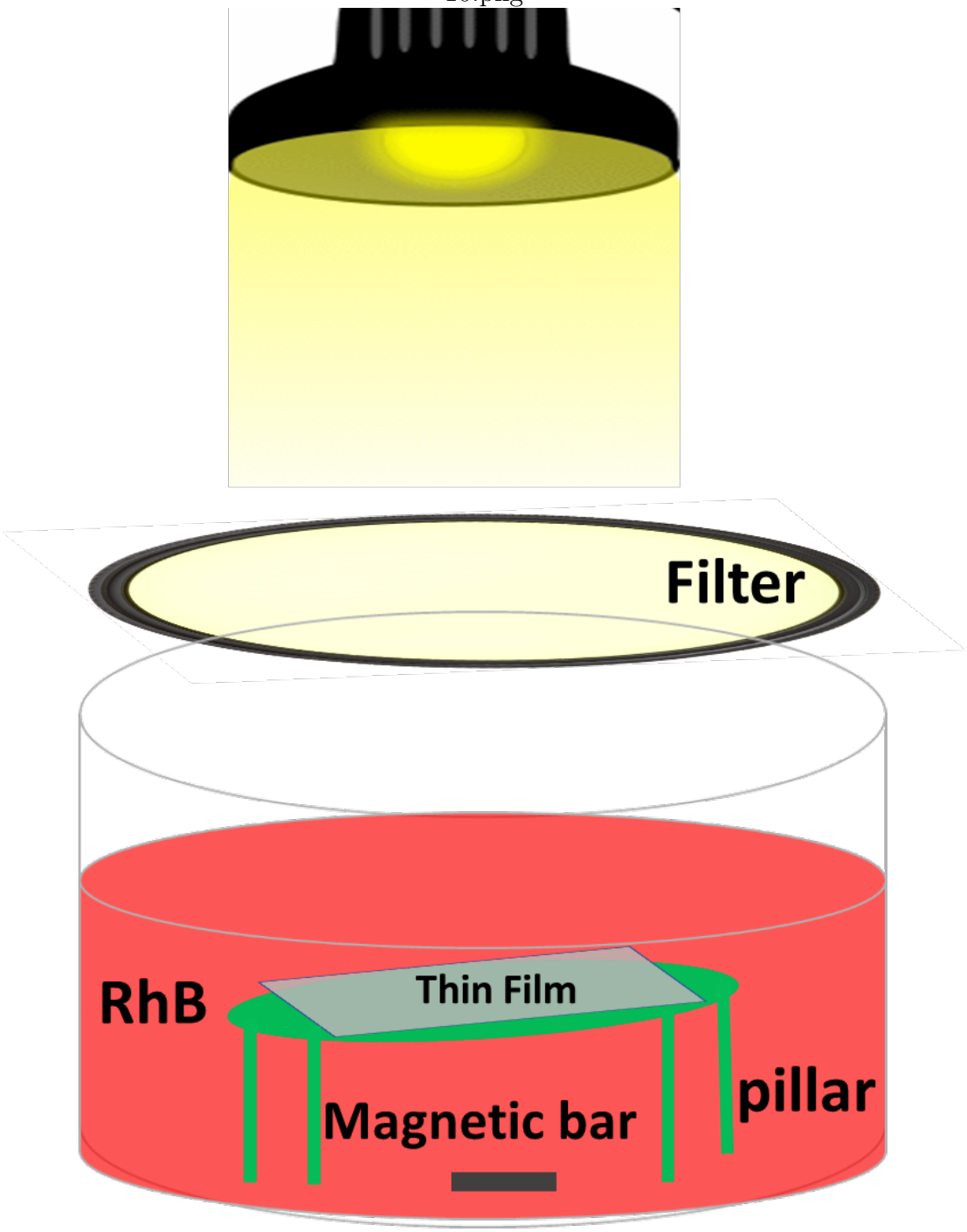

Figure 3.2: The degradation experiment setup

CHAPTER 4

RESULTS AND DISCUSION

4.1 rGO/CdS Results and descusion

4.1.1 Morphological and Structural Characterizations:

Figure 4.1 shows XRD patterns of as-purchased GO, as-purchased microstructured CdS and the synthesized CdS NPs and CdS/rGO. In Fig. 2a, the sharp (002) peak of GO, located at $2\theta = 11.8^o$, indicates a well-ordered, lamellar GO structure, which corresponds to the large an interlayer distance in GO due to the presence of intercalated H_2O molecules and various oxygen containing functional groups [29][76]. Figure 2b depicts the characteristic X-ray diffraction of microstructured CdS (commercial), where the observed diffraction peaks are according to the crystallographic planes of the hexagonal structure of CdS (ICDD PDF 80-0006) with the crystal lattice parameters of 4.12, 4.12 and 6.68 A [77][78]. The XRD peaks of CdS (figure 2c) after laser ablation are quite broad indicating that crystallite size of the as-prepared CdS NPs is relatively small compared with

that of the microstructured CdS. Figure 2d is the XRD pattern of CdS/rGO, where we can notice that the characteristic XRD pattern of CdS NPs is also retained to a great extent. It is reported that reduction of GO (in Cd/rGO) the oxygen containing functional groups are removed, leading to the narrowing down of the interlayer distance and consequently the XRD peak for rGO is expected to shift to $2\theta = 26^o$. However the absence of the typical XRD peak of rGO (in CdS/rGO) at 26^o is attributed to its small quantity of rGO in CdS/rGO and relatively low diffraction intensity [79].

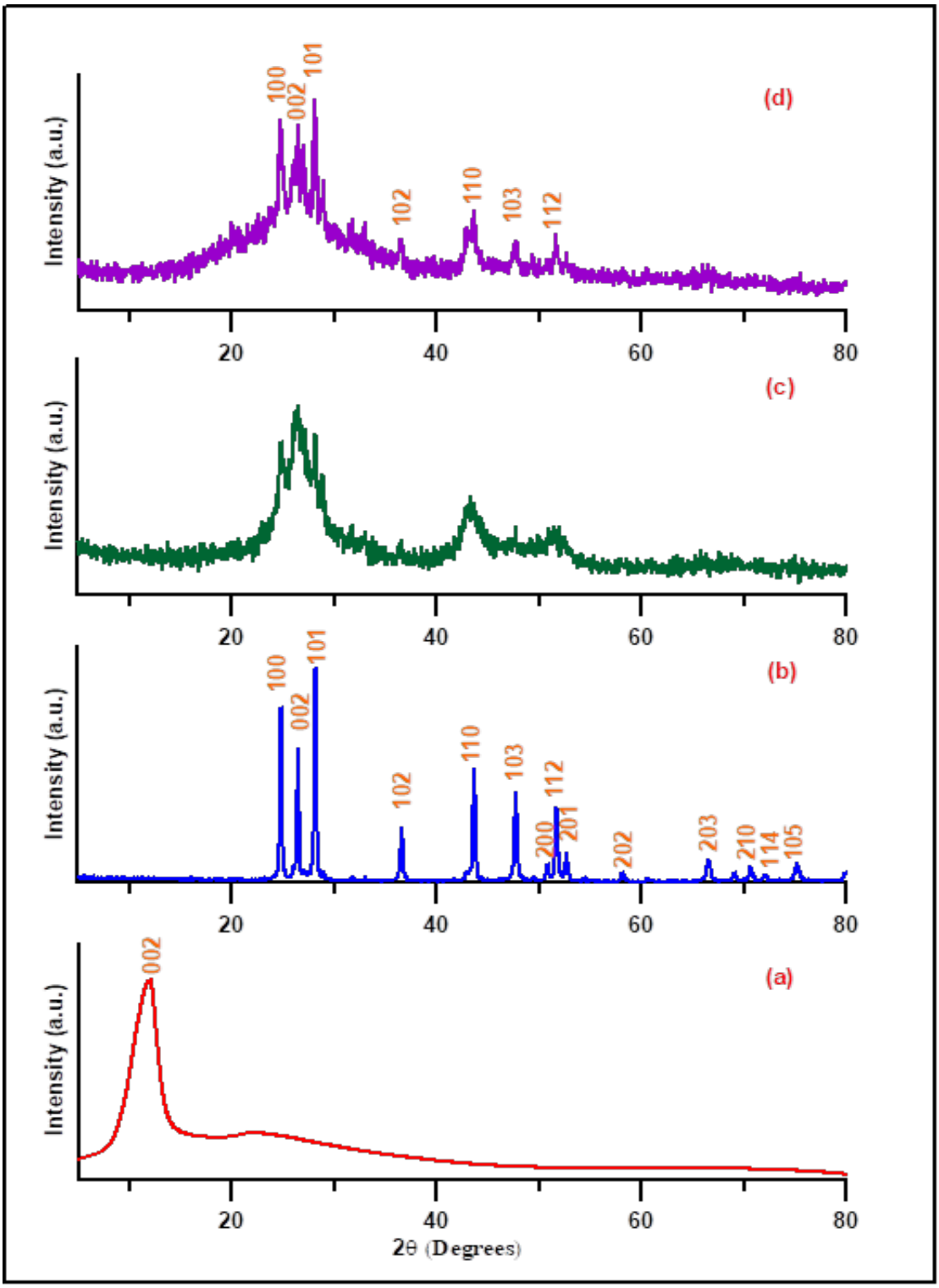

Figure 4.1: XRD patterns of (a) as purchased GO, (b) as purchased microstructured CdS, (c) the synthesized CdS NPs and (d) the synthesized rGO-CdS nanocopmposites.

Figure 4.2 appears the TEM images for as-synthesized CdS NPs and CdS/rGO, where the transformation of CdS from the microstructure to nanostructure due to pulsed laser ablation is evident. Although, the TEM image of CdS NPs in figure 3a shows a little aggregation with an average diameter around 50 nm, this aggregation as compared to CdS NPs synthesized by other methods is much lower [26][80]. Although, when GO was added during the pulsed ablation operation, the morphology of the CdS NPs became quite different, which is evident from the TEM image of CdS/rGO in figure 3b, where it is quite clear that CdS NPs were wrapped up closely with rGO sheets. When CdS/rGO nanocomposite is formed due to laser irradiation, the interfacial interactions were reinforced which paved a way for easy mobility of photo-induced electrons from CdS NPs to rGO, thereby increasing the transfer efficiency of the photo-induced charge carriers[25].

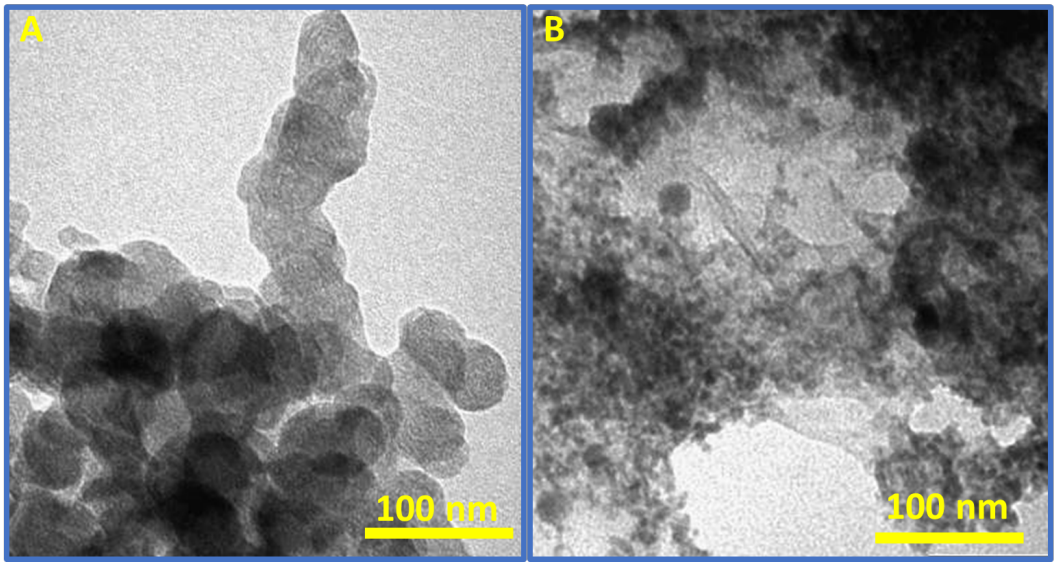

Figure 4.2: TEM images for (a) CdS nanostructure and (b) rGO-CdS

To verify the reduction of GO to rGO in the rGO/CdS nanocomposites, XPS analysis results are presented in Fig. 4.3a and b. As shown in Fig. 4.3(a), the survey spectra displays 2 peaks labelled therein, the peaks O1s indicating the dominant presence of O-containing groups. After irradiation, the intensity of O1s peak is decreased. Collectively, these results indicate the successful expulsion of the various oxygen-containing groups in GO by laser irradiation, transforming GO to rGO, the desired product. Also, we can understand the transformation of GO to rGO in the rGO-CdS due to laser irradiation, the chemical bonding between the carbon atoms and other atoms in GO and CdS/rGO sample were explored using X-ray photoelectron spectroscopy (XPS). Figure 4.4 a and b show the de-convoluted spectra of C1s for GO and CdS/rGO respectively. As displayed in fig 4.4a, the C1s spectra has four peaks at 283.28 eV, 285.38 eV, 287.08 eV and 282.78 eV which are due to carbon atoms in C-C (sp2 carbon), C-O(carbonyls), O-C=O(carboxyl) and C-OH (hydroxyls), respectively[24][81], which clearly denote the presence of oxygen containing functional groups in GO. On the other hand, in the de-convoluted C1s peak of CdS/rGO in figure 4.4b, the C-O and C-OH peaks completely vanished, while the C-C peaks experienced a reduction in its intensity. This observation suggests that oxygen-containing functional groups in GO was removed by laser irradiation. Thus, the laser irradiation was successfully used in transforming GO to reduced graphene oxide. It is worth mentioning that the presence of C-OH functional group facilitates the dispersion of nanocomposite material in aqueous solution, thus increasing the effectiveness of photo-catalyst

[24][1].

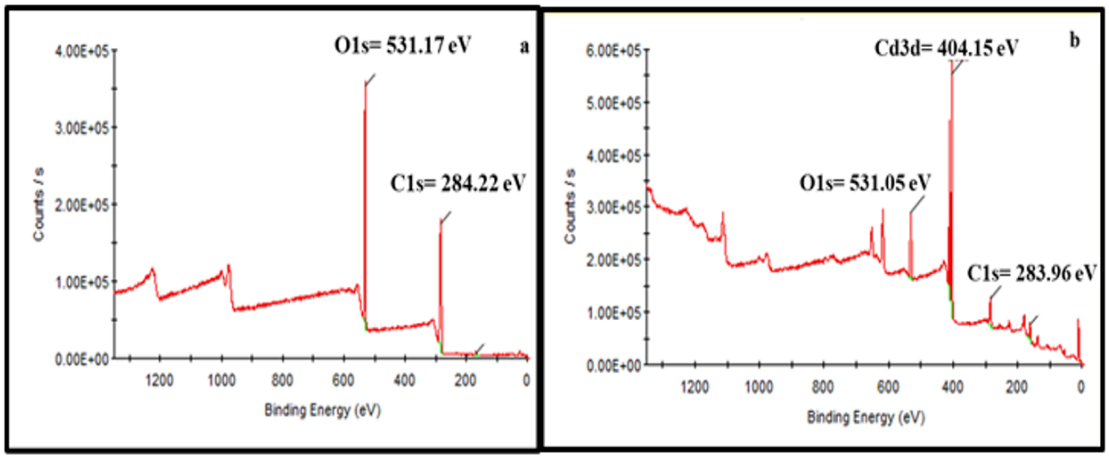

Figure 4.3: XPS survey spectrum of (a) GO and (b) CdS/rGO

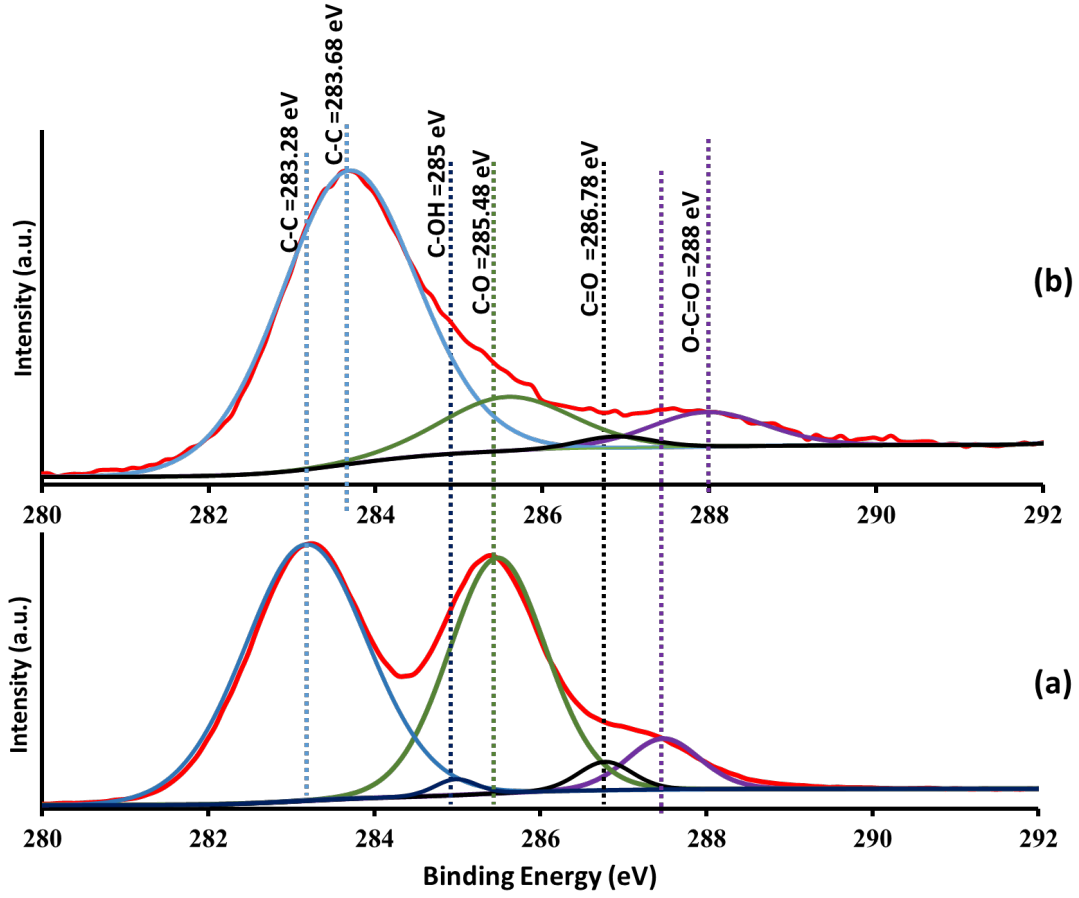

Figure 4.4: Deconvolution of C1s XPS peaks of carbon for (a) GO (b) rGO-CdS.

4.1.2 Optical Characterizations

The optical absorption spectra of rGO, CdS NPs and CdS/rGO are displayed in figure 4.5. From figure 4.5, it is quite obvious that with the introduction of rGO in CdS NPs, the light absorption is enhanced in the visible/IR spectral region as compared to the absorption of CdS NPs. In case of rGO, the absorbance peak is reported to be around 262 nm [82] [83] which is in agreement with our observation in figure 5. Although, CdS NPs has good characteristic optical absorption in the visible region of the spectrum, the enhanced absorption in the visible/IR spectral region due to the presence of rGO is an advantage for better harvesting of solar radiation for photo-catalytic applications [76][84]. In order to understand the effect of the presence of rGO in the reduction of charge recombination, we also carried out the PL spectra of CdS NP and CdS/rGO and these spectra are shown in figure 4.6, where figure 4.6 b (for CdS/ rGO) is enlarged 30 times to show the trend. The characteristic wide PL band centred around 515 nm in the visible region has its sources attributed to the radiative recombination of self-trapped excitons in CdS [13]. The enormous reduction of PL intensity in CdS/rGO indicates the efficient charge separation brought about by anchoring CdS on rGO sheets. This reduced charge recombination, coupled with the enhanced visible spectral absorptionimplies that CdS/rGO is expected to have much better photocatalytic performance compared to CdS NPs [15][25], which will be demonstrated in the following studies.

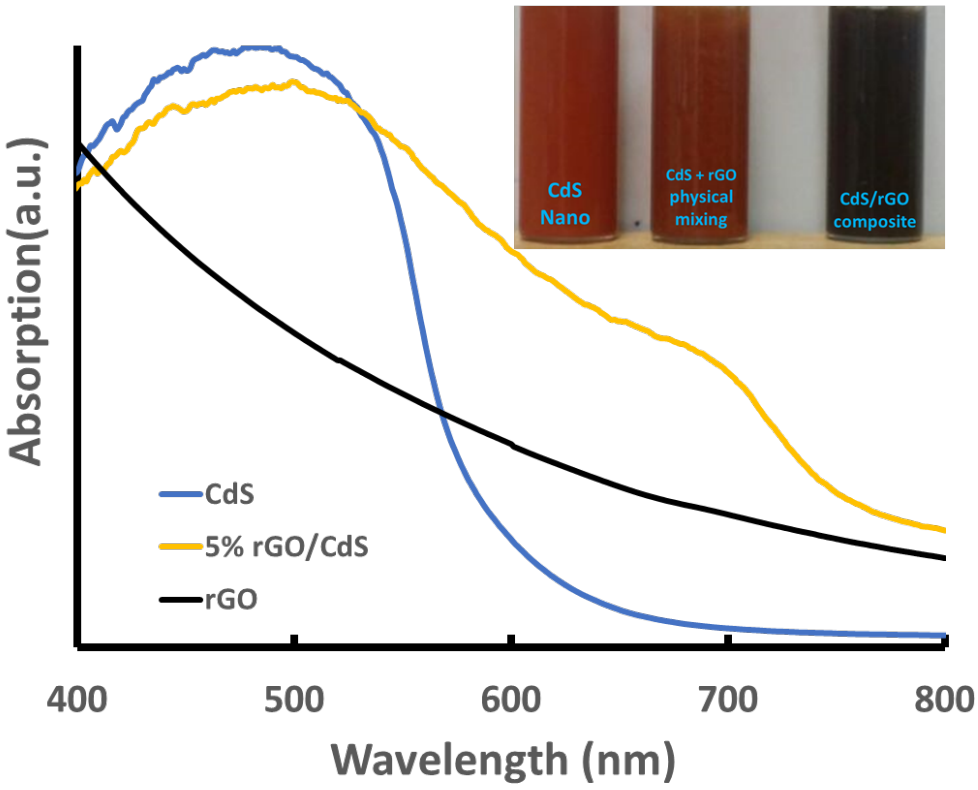

Figure 4.5: Optical absorption spectra of (a) CdS-NP and rGO-CdS.

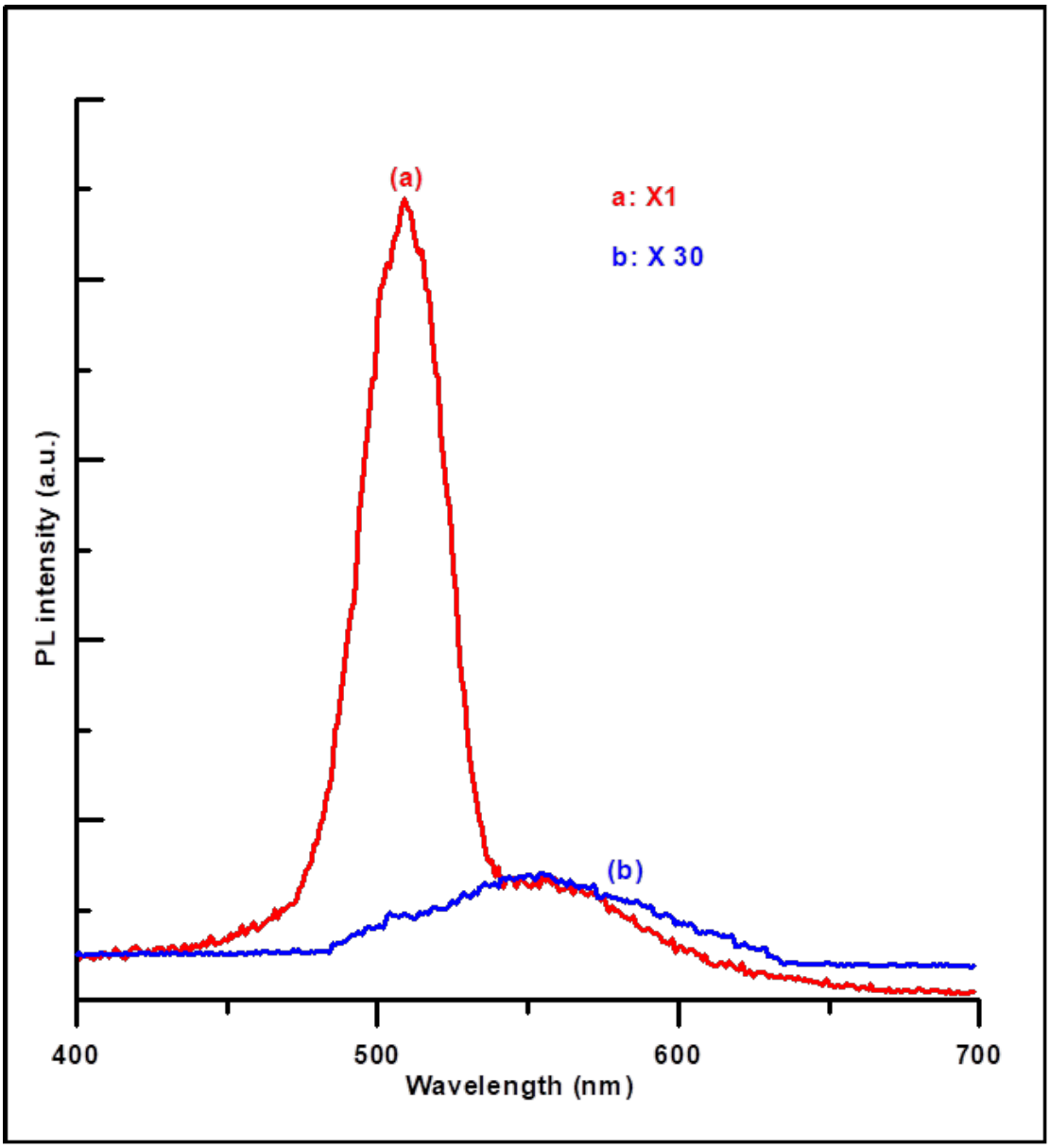

Figure 4.6: Photoluminescence spectra of (a) pure CdS, (b) rGO-CdS,-5% (30 times zoomed).

4.1.3 Photocatalytic degradation of MB dye using rGO/CdS

As the anchoring of CdS on rGO (in CdS/rGO) brought about the improvement of the key features, like increased surface area, reduced charge recombination, and

enhanced visible light absorption, which are essential for a good photo catalyst, we evaluated the photo-catalytic performance of CdS/rGO, by applying it as a photo-catalysts in the process of photocatalytic degradation of MB dye in the visible spectral region (wavelength > 420 nm). In addition to CdS/rGO, we also used pure CdS NPs and pure rGO as photocatalysts and the degradation curves with all these photo-catalysts are shown in figure 4.7, where C and C0 are the instantaneous and initial concentrations respectively. As it is evident from figure 4.7, no MB degradation was observed in the absence of a photo-catalyst, even after 150 minutes of visible light irradiation, but when pure rGO was used as a photo-catalyst, a slight degradation of MB under visible light is observable, and this can be attributed to the effect of high visible light absorption of rGO. It was estimated that CdS/rGO yielded a MB degradation efficiency of 77%, as compared to 28% MB degradation achieved by pure CdS NPs. The low degradation efficiency of CdS NPs could be due to the rapid recombination of photo-generated electron-hole pair as observed in the photoluminescence measurement. When CdS/rGO was used as a photo-catalyst for the degradation of MB dye, the efficiency of the degradation considerably enhanced as compared to that of pure CdS NPs, after 150 minutes of irradiation. The increased photo-catalytic degradation efficiency of CdS/rGO is as expected due to the increase of the surface area of the photo- catalyst, the enhancement in visible light absorption, and reduced electron hole recombination. The photo-catalytic degradation of MB dye using CdS/rGO starts as the visible light irradiates aqueous mixture of CdS/rGO and the MB dye. Following the

irradiation, electrons (e^-) are excited from the valence band to the conduction band of the CdS, leaving a hole (h^+) at the valence band. The conduction band and valence band for CdS with respect to vacuum level are -4.0 eV and -6.5 eV, respectively[85] and the work function of rGO is - 4.42 eV, which is below the conduction band of CdS NPs. Hence, anchoring of CdS NPs on rGO sheets enables the transfer of photo-excited electrons from the conduction band of CdS NPs to the rGO and delays the recombination of electron hole pairs [85].So it is clear that presence of rGO in CdS/rGO is so crucial that it inhibits the electron hole recombination, by taking the role of electron acceptor and transporter.

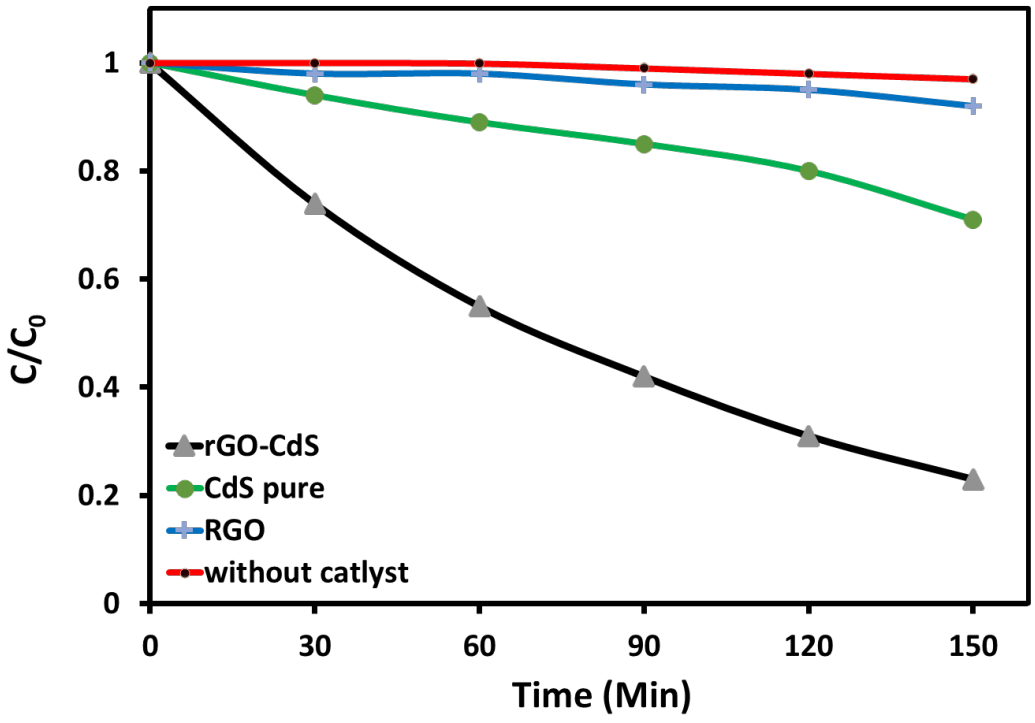

Figure 4.7: Photocatalytic degradation of Methylene blue dye (1) without catalyst (2) rGO, (3) CdS-NP (4) rGO-CdS-5%.

4.1.4 GO reduction and anchoring of CdS NPs by PLAL

In the first PLAL processes, microstructured CdS in water medium is converted into CdS NP, which is indicated by the change of colour in the suspension from orange to dark red after 20 minutes of irradiation by 532 nm laser beam with the pulse energy of 280 mJ. In the second PLAL process for producing CdS/rGO from CdS NP (produced in the first PLAL process) and GO in deionized water, these two chemical precursors reciprocate each other. Upon laser irradiation on CdS NPs, the electrons transfer from the conduction band (- 4 eV in vacuum level) to the valance band (-6.5 in vacuum level) [86]. The photo-generated electrons in the CdS help the reduction of GO in the water medium to form rGO and this rGO sheet in turn functions as a supporting matrix, co-catalyst, and electron acceptor for CdS. The formation of rGO from GO is indicated by the change of colour from brown to black as shown in the inset of figure 5, after 15 minutes of irradiation by 532 nm laser beam with the pulse energy of 280 mJ. Hence, the change in the absorption edge in the absorption spectra shown in figure 5, when CdS is anchored on the rGO sheets can be attributed to the visible manifestation of the change of colour depicted in the inset of figure 5 [87].Also the change of colour is attributed to the partial restoration of network within the carbon structure through chemical reduction of the GO sheets[88][89]. As CdS is inherently a visible light active material, electron hole pairs on the surface of CdS nanoparticle are generated by 532 nm laser and the presence of DI water in the suspension helps to minimize the electron hole recombination by scavenging photo-generated holes

to form hydroxyl radicals as shown in the chemical equation 1. The part of the photo-induced electrons on the surface of CdS NP mediates reduction reaction on GO to from rGO as shown in the chemical equation -2 and the and the remaining electrons are delocalized throughout the basal planes of GO sheets [87].

$$CdS + hV \longrightarrow CdS(e- + h^{+}) \longrightarrow^{H_2O} CdS(e) + OH + H^{+} \tag{4.1}$$

$$CdS(e) + GO \longrightarrow CdS + rGO \tag{4.2}$$

Now the CdS NPs (in CdS/rGO) are well spread on the rGO sheets, and this reduces the inherent aggregation of CdS NP and thereby helps to expand the surface area of the catalysts. Also this configuration along with the excess of electrons on the rGO sheets in the CdS/rGO helps to reduce the electron hole recombination during the actual photocatalytic reaction.

4.2 ZnO/RGO Results and Discussions

4.2.1 GO reduction and anchoring of ZnO NPs by PLAL

As mentioned earlier, the final composite ZnO/rGO is obtained through two PLAL processes with same experimental conditions. In the first PLAL process, microstructured Zn is mixed in the water medium and subjected to 40 minutes of UV irradiation with 355 nm laser beam with the pulse energy of 130 mJ. During

this process, Zn gets oxidized by the oxygen atoms, generated by the two step photo-dissociation of water molecules, resulting in the formation of ZnO NPs, which is indicated by the change of colour from black to white as shown in figure 4.8. The formation of ZnO NPs by PLAL process is described in the following chemical equations 1 to 3. [90].

$$H_2O + hv((laserat355nm) \longrightarrow H^+ + OH^- \tag{4.3}$$

$$OH^- + hv(laserat355nm) \longrightarrow O^* + H^* \tag{4.4}$$

$$Zn + O(laserat355nm) \longrightarrow ZnO \tag{4.5}$$

In the second PLAL process, ZnO NPs synthesized by the above process is mixed with the commercially available GO in deionized water medium and this mixture is subjected to the UV irradiation (355nm, 130 mJ pulse energy) for 15 minutes. During this process, electrons from the valance band of ZnO (- 4.2 eV in vacuum level) is transferred to the conduction band (- 7.5eV in vacuum level) and these photo-generated electrons mediate the reduction of GO to form rGO as shown in the chemical equations 4 and 5[91]. GO as such has many oxygen containing functional groups sandwiched between the GO sheets and through the reduction process some of these functional groups are removed and this leads to the enhancement of the electron conductivity in rGO sheets compared to that in GO sheets[50][51][52].On the other hand, rGO sheets functions as a supporting matrix, co-catalyst, and electron acceptor for ZnO. The formation of rGO from

GO by photo-reduction and the anchoring of ZnO on rGO sheets is manifested as the change in colour from white to brown as shown in figure 1 and also indicated in the absorption spectra that will be discussed in the next section. The change of colour is attributed to the partial restoration of network within the carbon structure through chemical reduction of the GO sheets[87][88][89].

$$ZnO + hV \longrightarrow ZnO(e - + h^{+})((H_2O)) \longrightarrow ZnO(e) + OH + H^{+} \tag{4.6}$$

$$ZnO(e) + GO \longrightarrow ZnO + rGO \tag{4.7}$$

Now the ZnO NPs (in ZnO/rGO) are well spread on the rGO sheets, and this reduces the inherent aggregation of ZnO NP and thereby helps to increase the surface area of the catalysts. Also this configuration along with the excess of electrons on the rGO sheets in the ZnO/rGO helps to reduce the electron hole recombination during the actual photo-catalytic reaction.

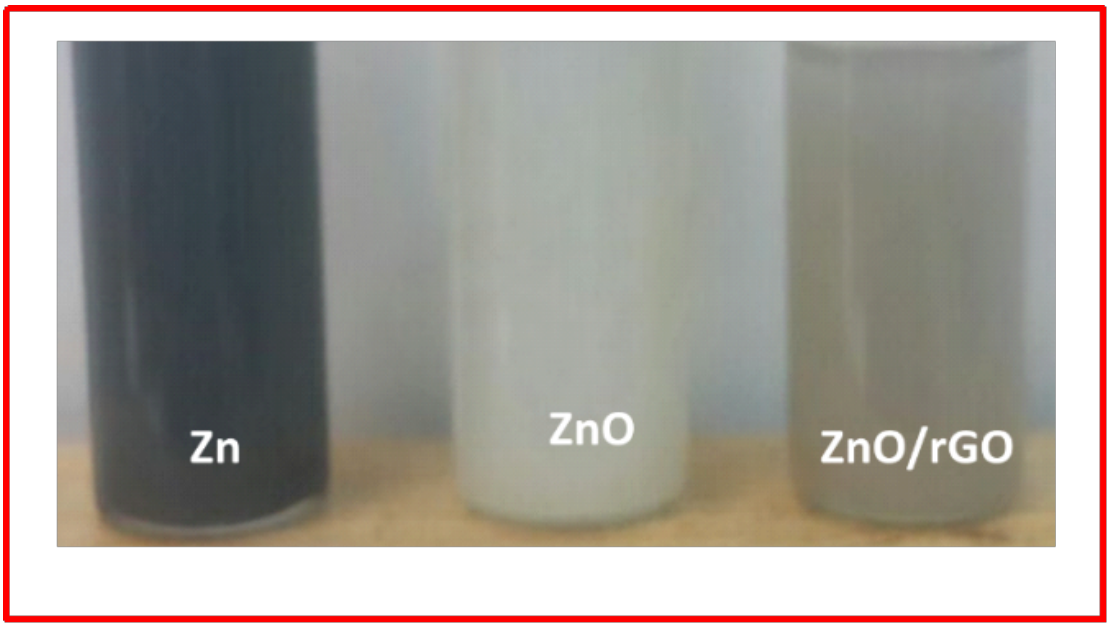

Figure 4.8: Change of colour during PLAL process from black for Zn (the starting material) to white for ZnO NP and further to light brown when ZnO is anchored on rGO.

4.2.2 Morphological and Structural Characterizations

The crystalline structures of as purchased micro structured GO (figure 4.9a), ZnO NPs (figure 4.9b) and the synthesized ZnO/rGO nanocomposites (figure 4.9c) were studied using XRD and the results are depicted in figure 2. The (002) diffraction peak of GO (figure 4.9a) at 2θ =11.81^o indicates a highly crystalline, lamellar GO structure and the appearance of the (002) peak at lower diffraction angle, compared to the peak position of graphite is attributed to the increased interlayer spacing, brought about by the intrusion of oxygen containing molecules [60][92]. The XRD of both ZnO and ZnO/rGO indicate the wurtzite ZnO structure

[42][33] and we can notice that even after the anchoring of ZnO on rGO (in ZnO/rGO), the XRD characteristics of ZnO is retained to a great extent. As more oxygen containing functional groups are removed through the reduction process, the interlayer distance between the GO sheets are expected to reduce leading to the shifting of (002) diffraction peak of GO to $2\theta = 26^o$. However the absence of the typical XRD peak of rGO (in ZnO/rGO) at 26o could be attributed to the lower content of rGO in ZnO/rGO and/or the anchoring of ZnO NPs on rGO inhibits the formation of stacks [60] .

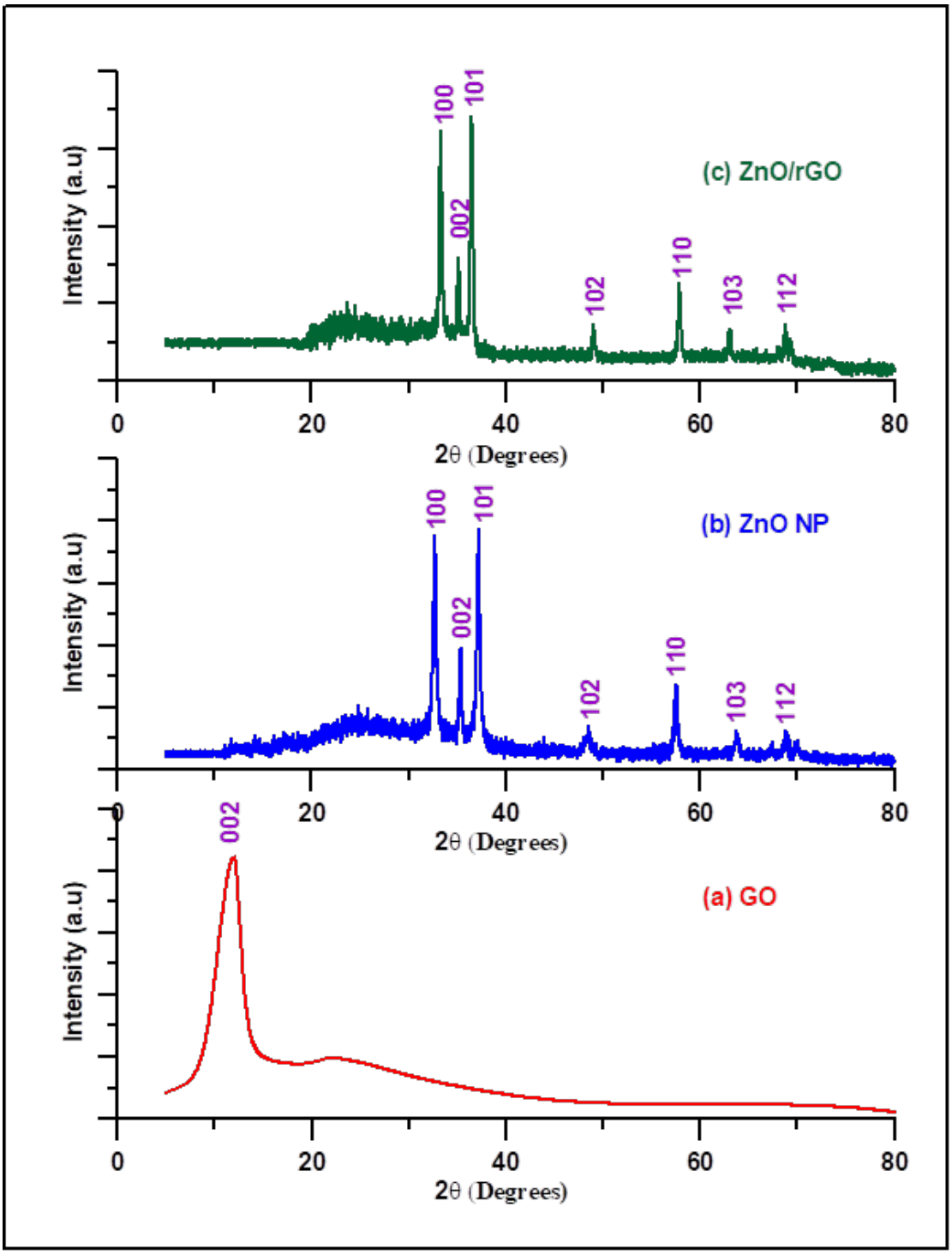

Figure 4.9: XRD pattern for (a) GO, (b) ZnO, and (c) ZnO/rGO nanocomposite.

Figure 4.10 shows the TEM images of ZnO NPs and ZnO/rGO synthesized by

PLAL and the image of ZnO NPs (figure 4.10a) clearly indicates that the pulsed laser ablation reduced the grain size of microstructured Zn (starting material) to the grain size of about 50 nm. The 50 nm grain size of ZnO indicates that a little bit of aggregation has occured in ZnO NPs, but this small aggregation in the PLAL method is much lower than shown by ZnO NPs synthesized using other methods [93][94].However, it is evident from the TEM image in figure 3b that when ZnO is anchored on the rGO, the ZnO NPs were wrapped up closely with rGO sheets, inhibiting the aggregation of the particle which leads to still smaller particle size. When ZnO/rGO nanocomposite is formed due to laser irradiation, the interfacial interactions were reinforced which paved a way for easy mobility of photo-induced electrons from ZnO NPs to rGO, thereby increasing the transfer efficiency of the photo-induced charge carriers[61][94].

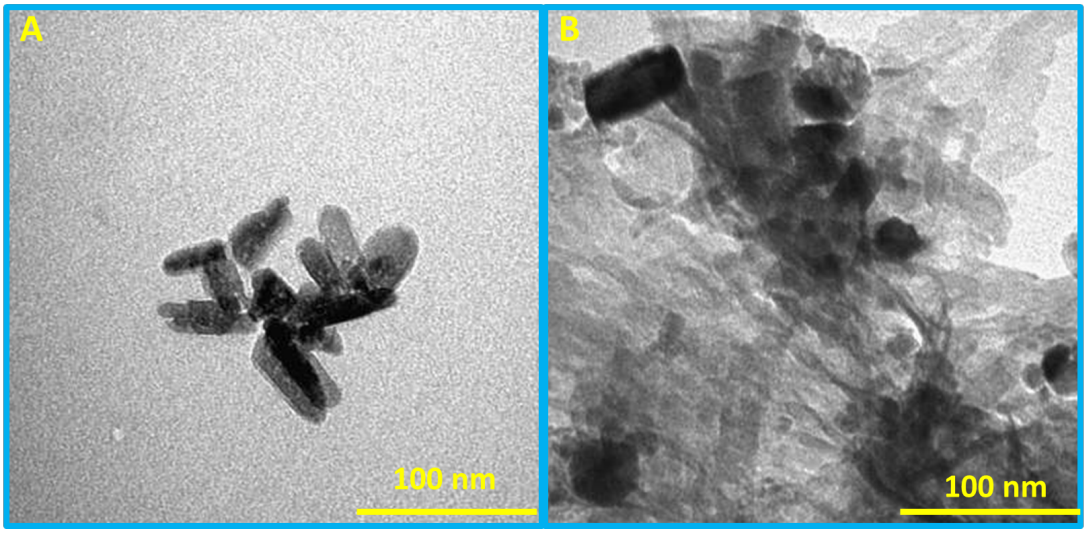

Figure 4.10: TEM images for (a) ZnO, and (b) ZnO/rGO nanocomposite.

To verify the reduction of GO to rGO in the rGO/CdS nanocomposites, XPS analysis results are presented in Fig. 4.11. As shown in Fig. 4.11(a), the survey spectra displays 2 peaks labelled therein, the peaks O1s indicating the dominant presence of O-containing groups. After irradiation, the intensity of O1s peak is decreased. Collectively, these results indicate the successful expulsion of the various oxygen-containing groups in GO by laser irradiation, transforming GO to rGO, the desired product. Also, reduction of GO mediated by the photo generated electrons in the ZnO to form rGO is evident from the X-ray photo-electron spectra (XPS), where the deconvoluted XPS peak of C1s for both GO and ZnO/rGO are displayed in figure 4.12a and figure 4.12b respectively. In the case of GO (figure 4.12a), the C1s peak has four components peaks cantered at 283.28 eV, 285.38 eV, 287.08 eV and 282.78 eV which are attributed to C-C (sp2 carbon), C-O(carbonyls), O-C=O(carboxyl) and C-OH (hydroxyls), respectively[95][24]. In the case C1s peak of ZnO/rGO in figure 4.12b, almost all the component peak due the oxygen containing groups (C-O. O-C=O and C-OH) present in figure 4a completely disappeared. Also, we noticed a new peak at 289.28 eV corresponding to the * satellite appears indicating the restoration of delocalized conjugated domain, while the C-C peaks experienced a reduction in its intensity. As it is clear from the XPs spectra, that the laser irradiation and the consequent production of photo generated electron in the ZnO NPs helps to eliminate oxygen containing functional groups in GO and transforming it into reduced graphene oxide (rGO). It is worth mentioning that the presence of very small amount of C-OH functional

group facilitates the dispersion of nanocomposite material in aqueous solution, thus increasing the effectiveness of photo-catalyst [95].

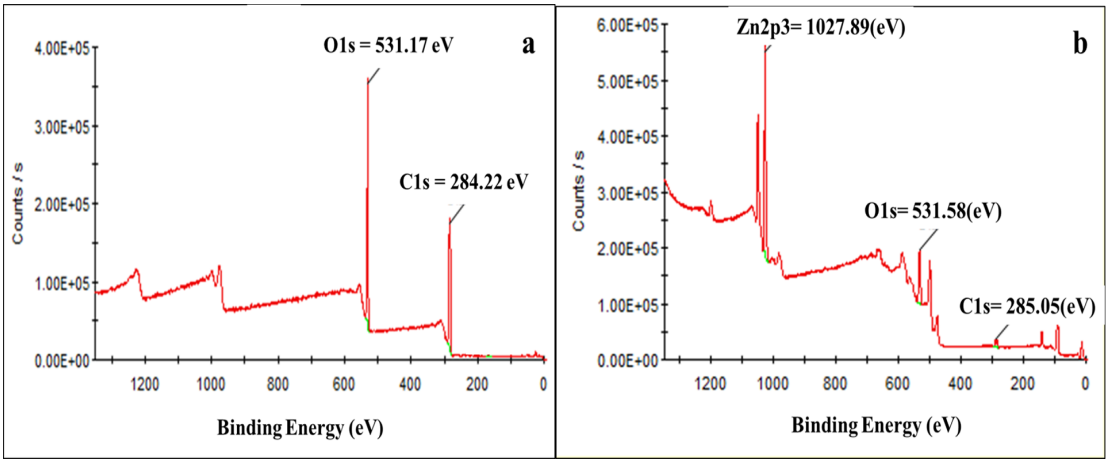

Figure 4.11: XPS survey spectrum of (a) GO and (b) ZnO/rGO

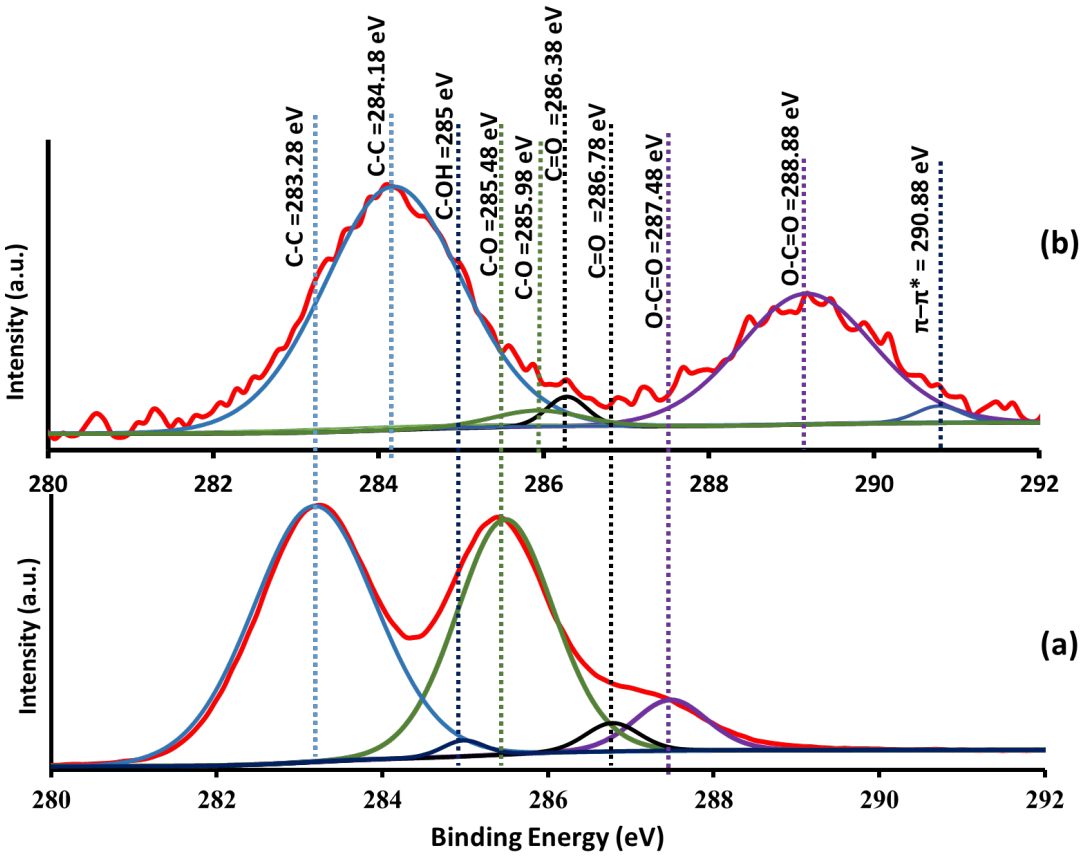

Figure 4.12: Deconvoluted C1s XPS component peaks for (a) GO and (b) ZnO/rGO

4.2.3 Optical Characterizations

The spectral absorbance and the band gap of ZnO and ZnO/rGO estimated by the diffuse reectance spectroscopy are shown in figure 4.13a and 4.13b respectively; where in the ordinal axes, reflectance is transformed into the absorbance equivalent KubelkaMunk function (F(R) = (1-R2)/2R) [95] [96]. In figure 4.13a, we can observe that the absorption edge is shifted slightly towards higher wavelength and also the absorbance intensity has enhanced in general and particularly in the visible spectral region. The band gap of these two materials were estimated using a Tauc plot, which is basically a plot of [F(R)*E]1/2 versus photon energy (E)[95] and shown in the inset of figure 5 for both ZnO and ZnO/rGO. Tauc plot shows a linear nature over a wide range when the exponent of the function in the ordinal axis of the plot is chosen to be 2, which is expected from the direct band gap nature of ZnO, and this nature is retained when ZnO is anchored on rGO sheet. According to the Tauc equation for the direct bad gap material,$(F(R) * E)^2 = A(E - E_(g))$,), the X intercept of the linear region of the plot is the band gap energy (Eg). The estimated band gap (Eg) for ZnO and ZnO/rGO from the Tauc plots are 3.15 eV and 3.04 eV respectively. This reduction in band gap after the formation of ZnO/rGO may be due to the interaction of ZnO and the -electron cloud of graphene sheets [95][97]. The reduction in the band gap brought about by anchoring of ZnO on rGO sheets amounts to the extension of the absorption of light in the visible region, which transforms ZnO/rGO into visible light active material which is not possible with pure ZnO.

[h!]

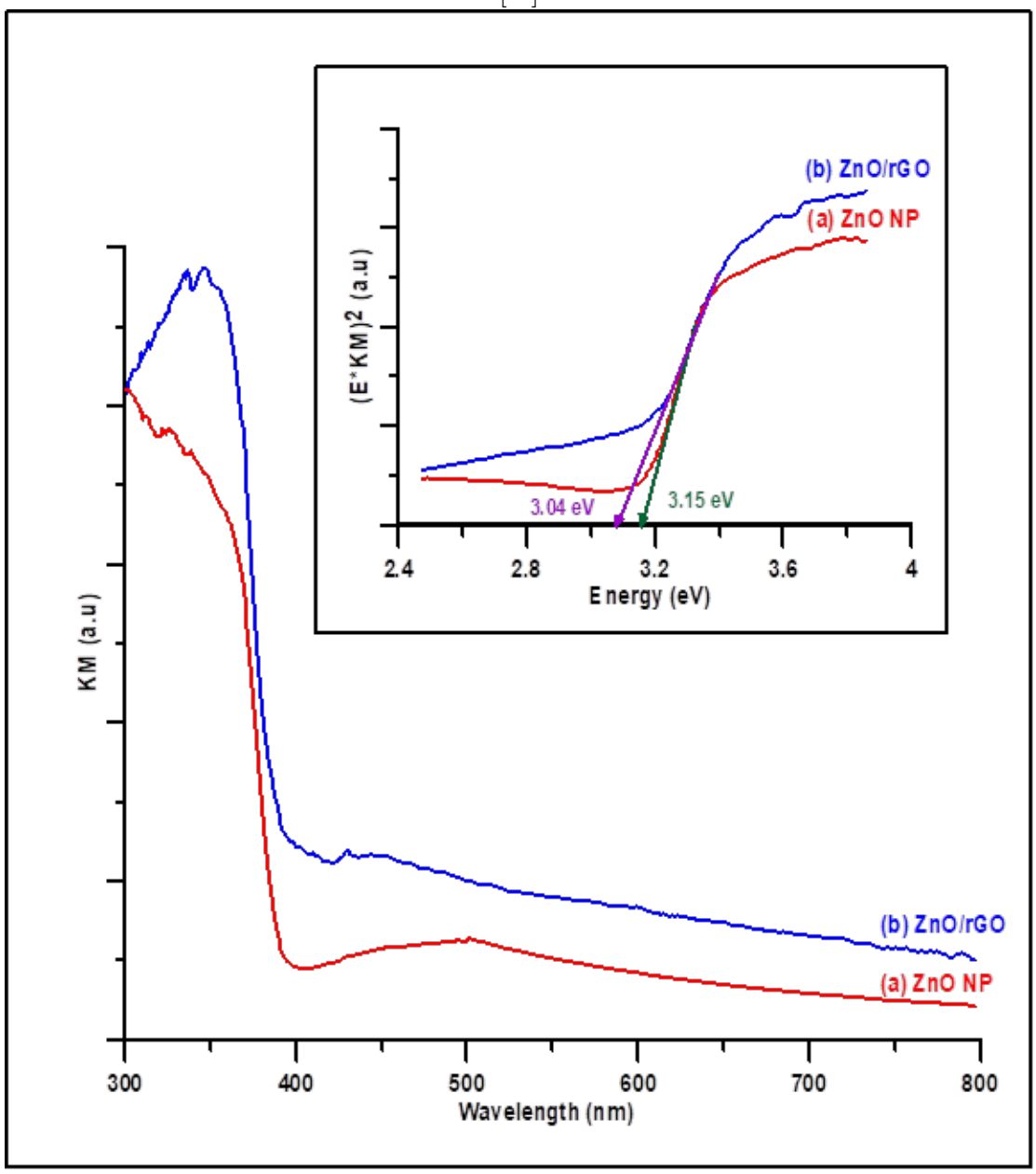

Figure 4.13: Absorption spectra for (a) ZnO, and (b) ZnO/rGO nanocomposite. The inset shows the Tauc plot and band gap energies of the same.

4.2.4 Photo-catalytic activity of synthesized materials

The synthesized ZnO NP and ZnO/rGO nanocomposites by PLAL method was tested,under the visible light radiation, for the photo-catalytic degradation of RhB dye , as ZnO/rGO shows an enhanced absorption in the visible region. In order to study the effect of photo-catalytic activity, we took the starting solution of RhB in DI water with the initial concentration of $C_0 = 10$ mg $L1$ and this solution in the presence of photo-catalytic film was subjected to visible light irradiation (> 390 nm) and during the irradiation process, a small amount of sample (1.5 ml) was taken at regular interval for the absorption studies to quantify their subsequent concentrations. The concentration of RhB present in water is quantified with the absorption peak at 554 nm, as the concentration of the dye is proportional to the absorption intensity of the RhB at this wavelength Figure 6 depicts the photo-catalytic degradation curves of RhB, presented as (C/C_0) versus time, where it is quite clear that in the situation that ther is no any photo-catalyst, the degradation of the dye does not take place even after 180 minutes of visible light irradiation. In figure 4.14, when ZnO and ZnO/rGO were used as a photo-catalyst to degrade RhB in water, appreciable dye degradation can be observed, with the manifestation of more steeper and more efficient degradation of RhB in water with ZnO/rGO as a photo-catalyst than with pure ZnO as a photo-catalyst under the same irradiation parameters. The photo-catalytic degradation efficiency (= (C_0-C) *100/C_0) of RhB in water with pure ZnO NP as a photo-catalyst is approximately 40% as compare to 86% with ZnO/rGO as photo-catalyst after

180 minutes of visible light irradiation. Also linearizing the decay curve, we estimated the rate of degradation (k) of RhB and the k values are 0.002 minute-1 and 0.011minutes-1 for ZnO and ZnO/rGO respectively. This means, whatever level of degradation achieved by ZnO/rGO in 180 minutes, it would take 985 minutes for the pure ZnO NP to achieve.

This enhanced photo-catalytic degradation efficiency (more than double) is obviously brought about by the improvements that took place on ZnO after it is anchored on rGO sheets. In the visible spectral region it is well known that ZnO is inactive , however a 40% degradation efficiency was achieved, because the visible light radiation we used ($>$ 390 nm) is close to the estimated band gap energy of ZnO NPs (3.15 eV equivalent to 392.0 nm). When ZnO is anchored on rGO sheets the visible light absorption characteristics of ZnO is changed as its band gap energy is reduced from 3.15 eV to 3.04 eV, which means the active visible spectral region of ZnO is extended all the way to 405 nm. The increase in the observed degradation efficiency of RhB in water using ZnO/rGO nanocomposite can be attributed to the extended and enhanced visible light absorption of the nanocomposite. Another reason for the increased efficiency of photo-catalytic degradation of RhB in water is due to the reduced recombination of photo-generated electron hole pairs. As the energy positions of the conduction band of ZnO (-4.05eV) and the Fermi level of rGO (4.42 eV))huang2014facile are so favorable that photo-generated electrons transfer from ZnO to rGO sheets, which is quite analogous to the mechanism where the noble metal doped semiconductor photo-catlysts,

the electrons are trapped by the noble metals. This charge separation promoted by rGO impedes the rapid recombination of light generated electron hole pairs, which results in the availability of more holes (h^+) in the valance band of ZnO to carry out the photo-catalytic degradation of RhB through direct oxidation. Moreover, rGO in the ZnO/rGO nanocomposite serves as a platform for the enhanced RhB adsorption on the catalytic surface and this along with the strong coupling between ZnO and rGO helps the degradation of the dye, with continuous replenishing of new RhB on to the catalytic surface for further degradation huang2014facilexu2011significantly. Also, it is clear from the TEM images in figure 3b, the ZnO NPs are wrapped up by the rGO sheet and this inhibits the inherent aggregation of ZnO NPs and makes more active ZnO surface area available for the interaction of dye. All the four positive factors discussed above, that were brought out by the anchoring of ZnO on rGO sheet by a single step PLAL process contribute favorably for the enhanced photo-catalytic degradation of RhB in the visible spectral region.

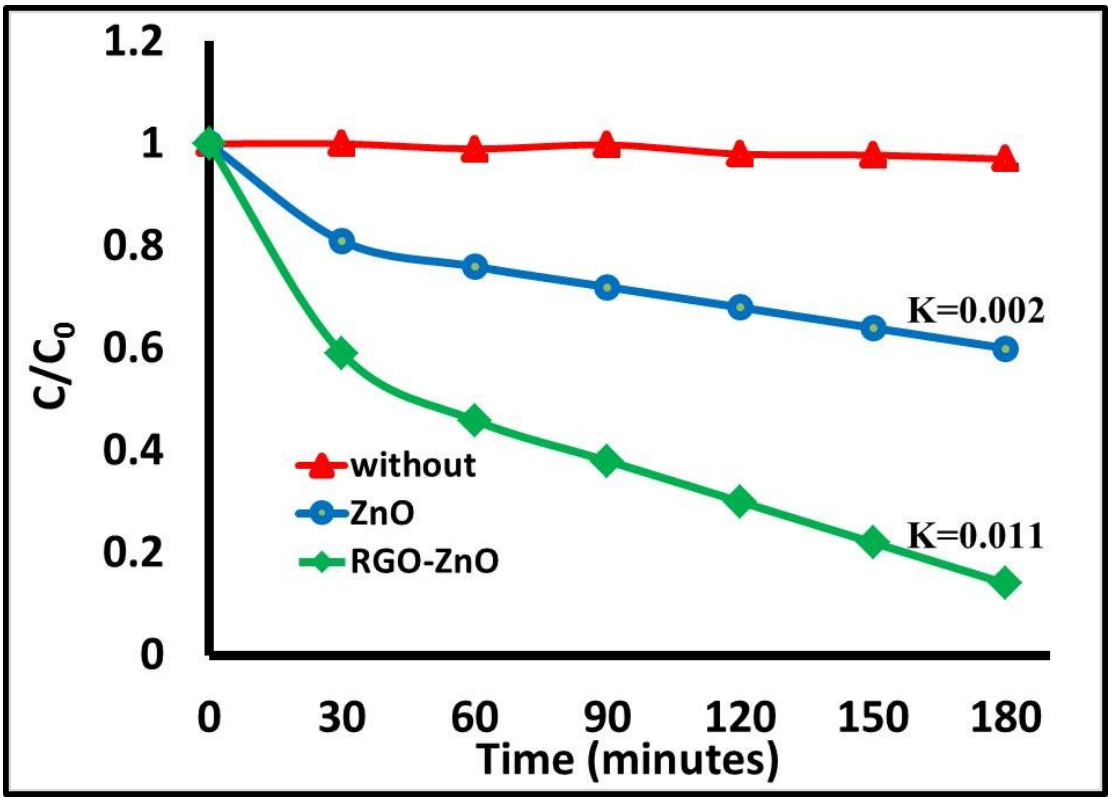

Figure 4.14: Photo-catalytic decay curve (ln(C/C0) vs time) for RhB with (a) No catalyst, (b) ZnO, and (c) ZnO/rGO nanocomposite. The inset shows the exponential decay.

CHAPTER 5

CONCLUSION

In this work, rGO/CdS and rGO/ZnO/ nanocomposite were prepared by the simple and one step process of pulsed laser ablation in liquid (PLAL) and this material was used as a photo-catalyst for the degradation of Rhodamine B dye and RhB in water. In this PLAL process, CdS, ZnO and graphene oxide (GO) in water were used as the starting materials and irradiated by high energy laser beam, the photo-generated electrons from CdS and ZnO mediated the reduction process in GO to produce reduced graphene oxide (rGO) and also in this process, CdS and ZnO nanoparticles get anchored on the produced rGO sheets. We carried out the morphological, elemental and optical characterization on this composite material and found that the presence of rGO in the rGO/CdS and ZnO/ rGO nanocomposite brought about the positive features, like enhanced and extended absorption in the visible spectral region, reduced recombination of photo-generated electron hole pairs, increased active catalytic surface area for more reactant catalyst interaction by reduced particle size, and increased adsorption. Encouraged by the

positive attributes brought out by the anchoring of CdS and ZnO on rGO, we applied rGO/CdS and ZnO/rGO naocomposites for the photo-catalytic degradation of MB dye and RhB in water and it was found that rGO/CdS and ZnO/rGO nano composite yielded a MB dye and RhB degradation efficiency of 77% and 86% regularly, as compared to the 28% and 40% degradation with pure CdS and ZnO NPs, which are quite expected from the above mentioned positive attributes brought about by the anchoring of CdS and ZnO on rGO.

REFERENCES

[1] X. Liu, Y. Li, J. Yang, B. Wang, M. Ma, F. Xu, R. Sun, and X. Zhang, "Enhanced photocatalytic activity of cds-decorated tio2/carbon core-shell microspheres derived from microcrystalline cellulose," *Materials*, vol. 9, no. 4, p. 245, 2016.

[2] R. C. Pawar, V. Khare, and C. S. Lee, "Hybrid photocatalysts using graphitic carbon nitride/cadmium sulfide/reduced graphene oxide (gc 3 n 4/cds/rgo) for superior photodegradation of organic pollutants under uv and visible light," *Dalton Transactions*, vol. 43, no. 33, pp. 12 514–12 527, 2014.

[3] O. IEA, "Energy and climate change, world energy outlook special report," 2015.

[4] S. Malato, P. Fernández-Ibáñez, M. I. Maldonado, J. Blanco, and W. Gernjak, "Decontamination and disinfection of water by solar photocatalysis: recent overview and trends," *Catalysis Today*, vol. 147, no. 1, pp. 1–59, 2009.

[5] V. Gupta *et al.*, "Application of low-cost adsorbents for dye removal–a review," *Journal of environmental management*, vol. 90, no. 8, pp. 2313–2342,

2009.

[6] P. Russo, L. DUrso, A. Hu, N. Zhou, and G. Compagnini, "In liquid laser treated graphene oxide for dye removal," *Applied Surface Science*, vol. 348, pp. 85–91, 2015.

[7] B. Hameed, A. M. Din, and A. Ahmad, "Adsorption of methylene blue onto bamboo-based activated carbon: kinetics and equilibrium studies," *Journal of hazardous materials*, vol. 141, no. 3, pp. 819–825, 2007.

[8] M. R. Hoffmann, S. T. Martin, W. Choi, and D. W. Bahnemann, "Environmental applications of semiconductor photocatalysis," *Chemical reviews*, vol. 95, no. 1, pp. 69–96, 1995.

[9] W. Hou and S. B. Cronin, "A review of surface plasmon resonance-enhanced photocatalysis," *Advanced Functional Materials*, vol. 23, no. 13, pp. 1612–1619, 2013.

[10] O. Alfano, D. Bahnemann, A. Cassano, R. Dillert, and R. Goslich, "Photocatalysis in water environments using artificial and solar light," *Catalysis today*, vol. 58, no. 2, pp. 199–230, 2000.

[11] X. Wang, K. Maeda, A. Thomas, K. Takanabe, G. Xin, J. M. Carlsson, K. Domen, and M. Antonietti, "A metal-free polymeric photocatalyst for hydrogen production from water under visible light," *Nature materials*, vol. 8, no. 1, pp. 76–80, 2009.

[12] T. Peng, K. Li, P. Zeng, Q. Zhang, and X. Zhang, "Enhanced photocatalytic hydrogen production over graphene oxide–cadmium sulfide nanocomposite under visible light irradiation," *The Journal of Physical Chemistry C*, vol. 116, no. 43, pp. 22 720–22 726, 2012.

[13] F. S. Hashim, M. A. Habeeb, and I. R. Ghanim, "Effect of zinc on structural and some optical properties of cds thin films," *Chemistry and Materials Research*, vol. 3, no. 12, 2013.

[14] J. Su, T. Zhang, Y. Li, Y. Chen, and M. Liu, "Photocatalytic activities of copper doped cadmium sulfide microspheres prepared by a facile ultrasonic spray-pyrolysis method," *Molecules*, vol. 21, no. 6, p. 735, 2016.

[15] A. Dumbrava, D. Berger, G. Prodan, F. Moscalu, and A. Diacon, "Facile synthesis, characterization and application of functionalized cadmium sulfide nanopowders," *Materials Chemistry and Physics*, vol. 173, pp. 70–77, 2016.

[16] M. E. Khan, M. M. Khan, and M. H. Cho, "Cds-graphene nanocomposite for efficient visible-light-driven photocatalytic and photoelectrochemical applications," *Journal of colloid and interface science*, vol. 482, pp. 221–232, 2016.

[17] X. Fu, Y. Zhang, P. Cao, H. Ma, P. Liu, L. He, J. Peng, J. Li, and M. Zhai, "Radiation synthesis of cds/reduced graphene oxide nanocomposites for visible-light-driven photocatalytic degradation of organic contaminant," *Radiation Physics and Chemistry*, vol. 123, pp. 79–86, 2016.

[18] F. Chen, D. Jia, X. Jin, Y. Cao, and A. Liu, "A general method for the synthesis of graphene oxide-metal sulfide composites with improved photocatalytic activities," *Dyes and Pigments*, vol. 125, pp. 142–150, 2016.

[19] Q. Xiang, J. Yu, and M. Jaroniec, "Graphene-based semiconductor photocatalysts," *Chemical Society Reviews*, vol. 41, no. 2, pp. 782–796, 2012.

[20] A. Wang, W. Yu, Y. Fang, Y. Song, D. Jia, L. Long, M. P. Cifuentes, M. G. Humphrey, and C. Zhang, "Facile hydrothermal synthesis and optical limiting properties of tio 2-reduced graphene oxide nanocomposites," *Carbon*, vol. 89, pp. 130–141, 2015.

[21] W. Gao, M. Wang, C. Ran, and L. Li, "Facile one-pot synthesis of mos 2 quantum dots–graphene–tio 2 composites for highly enhanced photocatalytic properties," *Chemical Communications*, vol. 51, no. 9, pp. 1709–1712, 2015.

[22] P. Zeng, Q. Zhang, T. Peng, and X. Zhang, "One-pot synthesis of reduced graphene oxide–cadmium sulfide nanocomposite and its photocatalytic hydrogen production," *Physical Chemistry Chemical Physics*, vol. 13, no. 48, pp. 21 496–21 502, 2011.

[23] R. C. Pawar and C. S. Lee, "Sensitization of cds nanoparticles onto reduced graphene oxide (rgo) fabricated by chemical bath deposition method for effective removal of cr (vi)," *Materials Chemistry and Physics*, vol. 141, no. 2, pp. 686–693, 2013.

[24] I. M. Leo, E. Soto, F. Vaquero, N. Mota, R. Navarro, and J. Fierro, "Influence of the reduction of graphene oxide (rgo) on the structure and photoactivity of cds-rgo hybrid systems," *International Journal of Hydrogen Energy*, vol. 42, no. 19, pp. 13 691–13 703, 2017.

[25] L. Zou, X. Wang, X. Xu, and H. Wang, "Reduced graphene oxide wrapped cds composites with enhanced photocatalytic performance and high stability," *Ceramics International*, vol. 42, no. 1, pp. 372–378, 2016.

[26] N. Meng, Y. Zhou, W. Nie, and P. Chen, "Synthesis of cds-decorated rgo nanocomposites by reflux condensation method and its improved photocatalytic activity," *Journal of Nanoparticle Research*, vol. 18, no. 8, p. 241, 2016.

[27] A. Hasani, H. S. Dehsari, A. A. Zarandi, A. Salehi, F. A. Taromi, and H. Kazeroni, "Visible light-assisted photoreduction of graphene oxide using cds nanoparticles and gas sensing properties," *Journal of Nanomaterials*, vol. 16, no. 1, p. 71, 2015.

[28] N. Zhang, M.-Q. Yang, Z.-R. Tang, and Y.-J. Xu, "Cds–graphene nanocomposites as visible light photocatalyst for redox reactions in water: a green route for selective transformation and environmental remediation," *Journal of catalysis*, vol. 303, pp. 60–69, 2013.

[29] X. Wang, H. Tian, Y. Yang, H. Wang, S. Wang, W. Zheng, and Y. Liu, "Reduced graphene oxide/cds for efficiently photocatalystic degradation of methylene blue," *Journal of Alloys and Compounds*, vol. 524, pp. 5–12, 2012.

[30] L. Wang, M. Wen, W. Wang, N. Momuinou, Z. Wang, and S. Li, "Photocatalytic degradation of organic pollutants using rgo supported tio 2-cds composite under visible light irradiation," *Journal of Alloys and Compounds*, vol. 683, pp. 318–328, 2016.

[31] M.-Q. Yang and Y.-J. Xu, "Selective photoredox using graphene-based composite photocatalysts," *Physical Chemistry Chemical Physics*, vol. 15, no. 44, pp. 19 102–19 118, 2013.

[32] C. Han, M.-Q. Yang, B. Weng, and Y.-J. Xu, "Improving the photocatalytic activity and anti-photocorrosion of semiconductor zno by coupling with versatile carbon," *Physical Chemistry Chemical Physics*, vol. 16, no. 32, pp. 16 891–16 903, 2014.

[33] M.-C. Hung, S.-Y. Yuan, C.-C. Hung, C.-L. Cheng, H.-C. Ho, and T.-H. Ko, "Effectiveness of zno/carbon-based material as a catalyst for photodegradation of acrolein," *Carbon*, vol. 66, pp. 93–104, 2014.

[34] H. Yao, F. Li, J. Lutkenhaus, M. Kotaki, and H.-J. Sue, "High-performance photocatalyst based on nanosized zno-reduced graphene oxide hybrid for removal of rhodamine b under visible light irradiation," *AIMS Mater Sci*, vol. 3, pp. 1410–1425, 2016.

[35] L. Zhang, H. Cheng, R. Zong, and Y. Zhu, "Photocorrosion suppression of zno nanoparticles via hybridization with graphite-like carbon and enhanced

photocatalytic activity," *The Journal of Physical Chemistry C*, vol. 113, no. 6, pp. 2368–2374, 2009.

[36] S. Cho, J.-W. Jang, J. Kim, J. S. Lee, W. Choi, and K.-H. Lee, "Three-dimensional type ii zno/znse heterostructures and their visible light photocatalytic activities," *Langmuir*, vol. 27, no. 16, pp. 10 243–10 250, 2011.

[37] S. Anandan, N. Ohashi, and M. Miyauchi, "Zno-based visible-light photocatalyst: Band-gap engineering and multi-electron reduction by co-catalyst," *Applied Catalysis B: Environmental*, vol. 100, no. 3, pp. 502–509, 2010.

[38] K. M. Lee, C. W. Lai, K. S. Ngai, and J. C. Juan, "Recent developments of zinc oxide based photocatalyst in water treatment technology: a review," *Water research*, vol. 88, pp. 428–448, 2016.

[39] F. Hussin, H. O. Lintang, and L. Yuliati, "Enhanced activity of c3n4 with addition of zno for photocatalytic removal of phenol under visible light," *Malaysian Journal of Analytical Sciences*, vol. 20, no. 1, pp. 102–110, 2016.

[40] V. Etacheri, R. Roshan, and V. Kumar, "Mg-doped zno nanoparticles for efficient sunlight-driven photocatalysis," *ACS applied materials & interfaces*, vol. 4, no. 5, pp. 2717–2725, 2012.

[41] R. Mohan, K. Krishnamoorthy, and S.-J. Kim, "Enhanced photocatalytic activity of cu-doped zno nanorods," *Solid State Communications*, vol. 152, no. 5, pp. 375–380, 2012.

[42] R. Georgekutty, M. K. Seery, and S. C. Pillai, "A highly efficient ag-zno photocatalyst: synthesis, properties, and mechanism," 2008.

[43] M. T. Uddin, Y. Nicolas, C. Olivier, T. Toupance, L. Servant, M. M. Muller, H.-J. Kleebe, J. Ziegler, and W. Jaegermann, "Nanostructured sno2–zno heterojunction photocatalysts showing enhanced photocatalytic activity for the degradation of organic dyes," *Inorganic chemistry*, vol. 51, no. 14, pp. 7764–7773, 2012.

[44] D. Jassby, J. Farner Budarz, and M. Wiesner, "Impact of aggregate size and structure on the photocatalytic properties of tio2 and zno nanoparticles," *Environmental science & technology*, vol. 46, no. 13, pp. 6934–6941, 2012.

[45] M. A. Rafiee, J. Rafiee, Z. Wang, H. Song, Z.-Z. Yu, and N. Koratkar, "Enhanced mechanical properties of nanocomposites at low graphene content," *ACS nano*, vol. 3, no. 12, pp. 3884–3890, 2009.

[46] A. A. Balandin, S. Ghosh, W. Bao, I. Calizo, D. Teweldebrhan, F. Miao, and C. N. Lau, "Superior thermal conductivity of single-layer graphene," *Nano letters*, vol. 8, no. 3, pp. 902–907, 2008.

[47] Z.-S. Wu, W. Ren, L. Gao, J. Zhao, Z. Chen, B. Liu, D. Tang, B. Yu, C. Jiang, and H.-M. Cheng, "Synthesis of graphene sheets with high electrical conductivity and good thermal stability by hydrogen arc discharge exfoliation," *ACS nano*, vol. 3, no. 2, pp. 411–417, 2009.

[48] M. A. Worsley, S. O. Kucheyev, H. E. Mason, M. D. Merrill, B. P. Mayer, J. Lewicki, C. A. Valdez, M. E. Suss, M. Stadermann, P. J. Pauzauskie *et al.*, "Mechanically robust 3d graphene macroassembly with high surface area," *Chemical Communications*, vol. 48, no. 67, pp. 8428–8430, 2012.

[49] K. I. Bolotin, K. Sikes, Z. Jiang, M. Klima, G. Fudenberg, J. Hone, P. Kim, and H. Stormer, "Ultrahigh electron mobility in suspended graphene," *Solid State Communications*, vol. 146, no. 9, pp. 351–355, 2008.

[50] F. Hussin, H. O. Lintang, S. L. Lee, and L. Yuliati, "Photocatalytic synthesis of reduced graphene oxide-zinc oxide: Effects of light intensity and exposure time," *Journal of Photochemistry and Photobiology A: Chemistry*, vol. 340, pp. 128–135, 2017.

[51] Y. Min, K. Zhang, W. Zhao, F. Zheng, Y. Chen, and Y. Zhang, "Enhanced chemical interaction between tio 2 and graphene oxide for photocatalytic decolorization of methylene blue," *Chemical Engineering Journal*, vol. 193, pp. 203–210, 2012.

[52] B. Li, T. Liu, Y. Wang, and Z. Wang, "Zno/graphene-oxide nanocomposite with remarkably enhanced visible-light-driven photocatalytic performance," *Journal of colloid and interface science*, vol. 377, no. 1, pp. 114–121, 2012.

[53] X. Zhou, T. Shi, and H. Zhou, "Hydrothermal preparation of zno-reduced graphene oxide hybrid with high performance in photocatalytic degradation," *Applied surface science*, vol. 258, no. 17, pp. 6204–6211, 2012.

[54] T. Lv, L. Pan, X. Liu, T. Lu, G. Zhu, and Z. Sun, "Enhanced photocatalytic degradation of methylene blue by zno-reduced graphene oxide composite synthesized via microwave-assisted reaction," *Journal of Alloys and Compounds*, vol. 509, no. 41, pp. 10 086–10 091, 2011.

[55] N. Kumar, A. K. Srivastava, H. S. Patel, B. K. Gupta, and G. D. Varma, "Facile synthesis of zno–reduced graphene oxide nanocomposites for no2 gas sensing applications," *European Journal of Inorganic Chemistry*, vol. 2015, no. 11, pp. 1912–1923, 2015.

[56] W. Feng, Y. Wang, J. Chen, L. Wang, L. Guo, J. Ouyang, D. Jia, and Y. Zhou, "Reduced graphene oxide decorated with in-situ growing zno nanocrystals: facile synthesis and enhanced microwave absorption properties," *Carbon*, vol. 108, pp. 52–60, 2016.

[57] Z. Zhan, L. Zheng, Y. Pan, G. Sun, and L. Li, "Self-powered, visible-light photodetector based on thermally reduced graphene oxide–zno (rgo–zno) hybrid nanostructure," *Journal of Materials Chemistry*, vol. 22, no. 6, pp. 2589–2595, 2012.

[58] B. Weng, M.-Q. Yang, N. Zhang, and Y.-J. Xu, "Toward the enhanced photoactivity and photostability of zno nanospheres via intimate surface coating with reduced graphene oxide," *Journal of Materials Chemistry A*, vol. 2, no. 24, pp. 9380–9389, 2014.

[59] A. A. Ashkarran and B. Mohammadi, "Zno nanoparticles decorated on graphene sheets through liquid arc discharge approach with enhanced photocatalytic performance under visible-light," *Applied Surface Science*, vol. 342, pp. 112–119, 2015.

[60] K. Huang, Y. Li, S. Lin, C. Liang, H. Wang, C. Ye, Y. Wang, R. Zhang, D. Fan, H. Yang *et al.*, "A facile route to reduced graphene oxide–zinc oxide nanorod composites with enhanced photocatalytic activity," *Powder technology*, vol. 257, pp. 113–119, 2014.

[61] N. Song, H. Fan, and H. Tian, "Reduced graphene oxide/zno nanohybrids: metallic zn powder induced one-step synthesis for enhanced photocurrent and photocatalytic response," *Applied Surface Science*, vol. 353, pp. 580–587, 2015.

[62] Q.-P. Luo, X.-Y. Yu, B.-X. Lei, H.-Y. Chen, D.-B. Kuang, and C.-Y. Su, "Reduced graphene oxide-hierarchical zno hollow sphere composites with enhanced photocurrent and photocatalytic activity," *The Journal of Physical Chemistry C*, vol. 116, no. 14, pp. 8111–8117, 2012.

[63] A. Marlinda, N. Huang, M. Muhamad, M. An'Amt, B. Chang, N. Yusoff, I. Harrison, H. Lim, C. H. Chia, and S. V. Kumar, "Highly efficient preparation of zno nanorods decorated reduced graphene oxide nanocomposites," *Materials Letters*, vol. 80, pp. 9–12, 2012.

[64] D. Krishnan, F. Kim, J. Luo, R. Cruz-Silva, L. J. Cote, H. D. Jang, and J. Huang, "Energetic graphene oxide: challenges and opportunities," *Nano today*, vol. 7, no. 2, pp. 137–152, 2012.

[65] J. Wang, S. Liang, L. Ma, S. Ding, X. Yu, L. Zhou, and Q. Wang, "One-pot synthesis of cds–reduced graphene oxide 3d composites with enhanced photocatalytic properties," *CrystEngComm*, vol. 16, no. 3, pp. 399–405, 2014.

[66] H. Liu, T. Lv, X. Wu, C. Zhu, and Z. Zhu, "Preparation and enhanced photocatalytic activity of cds@ rgo core–shell structural microspheres," *Applied Surface Science*, vol. 305, pp. 242–246, 2014.

[67] A. Ye, W. Fan, Q. Zhang, W. Deng, and Y. Wang, "Cds–graphene and cds–cnt nanocomposites as visible-light photocatalysts for hydrogen evolution and organic dye degradation," *Catalysis Science & Technology*, vol. 2, no. 5, pp. 969–978, 2012.

[68] P. V. More, C. Hiragond, A. Dey, and P. K. Khanna, "Band engineered p-type rgo–cds–pani ternary nanocomposites for thermoelectric applications," *Sustainable Energy & Fuels*, vol. 1, no. 8, pp. 1766–1773, 2017.

[69] K. Chakraborty, S. Ibrahim, P. Das, S. Ghosh, and T. Pal, "Reduced graphene oxide-cds nanocomposite with enhanced photocatalytic 4-nitrophenol degradation," in *AIP Conference Proceedings*, vol. 1832, no. 1. AIP Publishing, 2017, p. 050077.

[70] Y.-C. Lin, D.-C. Tsai, Z.-C. Chang, and F.-S. Shieu, "Ultrasonic chemical synthesis of cds-reduced graphene oxide nanocomposites with an enhanced visible light photoactivity," *Applied Surface Science*, 2018.

[71] A. Singh and A. Sinha, "Active cds/rgo photocatalyst by a high temperature gas-solid reaction for hydrogen production by splitting of water," *Applied Surface Science*, vol. 430, pp. 184–197, 2018.

[72] J. Qin, X. Zhang, C. Yang, M. Cao, M. Ma, and R. Liu, "Zno microspheres-reduced graphene oxide nanocomposite for photocatalytic degradation of methylene blue dye," *Applied Surface Science*, vol. 392, pp. 196–203, 2017.

[73] H. Moussa, E. Girot, K. Mozet, H. Alem, G. Medjahdi, and R. Schneider, "Zno rods/reduced graphene oxide composites prepared via a solvothermal reaction for efficient sunlight-driven photocatalysis," *Applied Catalysis B: Environmental*, vol. 185, pp. 11–21, 2016.

[74] C. B. Ong, A. W. Mohammad, L. Y. Ng, E. Mahmoudi, S. Azizkhani, and N. H. H. Hairom, "Solar photocatalytic and surface enhancement of zno/rgo nanocomposite: Degradation of perfluorooctanoic acid and dye," *Process Safety and Environmental Protection*, vol. 112, pp. 298–307, 2017.

[75] Y. T. Li, J. M. Xu, Z. J. Tang, T. T. Xu, and X. J. Li, "Nearly white light photoluminescence from zno/rgo nanocomposite prepared by a one-step hydrothermal method," *Journal of Alloys and Compounds*, vol. 715, pp. 122–128, 2017.

[76] N. Jiang, Z. Xiu, Z. Xie, H. Li, G. Zhao, W. Wang, Y. Wu, and X. Hao, "Reduced graphene oxide–cds nanocomposites with enhanced visible-light photoactivity synthesized using ionic-liquid precursors," *New Journal of Chemistry*, vol. 38, no. 9, pp. 4312–4320, 2014.

[77] L. Zou, X. Wang, X. Xu, and H. Wang, "Reduced graphene oxide wrapped CdS composites with enhanced photocatalytic performance and high stability," *Ceramics International*, vol. 42, no. 1, pp. 372–378, 2015.

[78] C.-H. Deng, J.-L. Gong, G.-M. Zeng, Y. Jiang, C. Zhang, H.-Y. Liu, and S.-Y. Huan, "Graphene–cds nanocomposite inactivation performance toward escherichia coli in the presence of humic acid under visible light irradiation," *Chemical Engineering Journal*, vol. 284, pp. 41–53, 2016.

[79] I. Ibrahim, H. Lim, N. Huang, and A. Pandikumar, "Cadmium sulphide-reduced graphene oxide-modified photoelectrode-based photoelectrochemical sensing platform for copper (ii) ions," *PloS one*, vol. 11, no. 5, p. e0154557, 2016.

[80] A. M. Darwish, W. H. Eisa, A. A. Shabaka, and M. H. Talaat, "Synthesis of nano-cadmium sulfide by pulsed laser ablation in liquid environment," *Spectroscopy Letters*, vol. 48, no. 9, pp. 638–645, 2015.

[81] H. He, H. Wang, K. Li, J. Zhu, J. Liu, X. Meng, X. Shen, X. Zeng, and W. Cai, "Green and tunable decoration of graphene with spherical nanopar-

ticles based on laser ablation in water: A case of ag nanoparticle/graphene oxide sheet composites," *Langmuir*, vol. 32, no. 7, pp. 1667–1673, 2016.

[82] X. Liu, L. Pan, T. Lv, G. Zhu, Z. Sun, and C. Sun, "Microwave-assisted synthesis of cds–reduced graphene oxide composites for photocatalytic reduction of cr (vi)," *Chemical Communications*, vol. 47, no. 43, pp. 11 984–11 986, 2011.

[83] J. Wu, S. Bai, X. Shen, and L. Jiang, "Preparation and characterization of graphene/cds nanocomposites," *Applied Surface Science*, vol. 257, no. 3, pp. 747–751, 2010.

[84] X.-Y. Zhang, H.-P. Li, X.-L. Cui, and Y. Lin, "Graphene/tio 2 nanocomposites: synthesis, characterization and application in hydrogen evolution from water photocatalytic splitting," *Journal of Materials Chemistry*, vol. 20, no. 14, pp. 2801–2806, 2010.

[85] X. An, X. Yu, C. Y. Jimmy, and G. Zhang, "Cds nanorods/reduced graphene oxide nanocomposites for photocatalysis and electrochemical sensing," *Journal of Materials Chemistry A*, vol. 1, no. 16, pp. 5158–5164, 2013.

[86] P. Huo, M. Zhou, Y. Tang, X. Liu, C. Ma, L. Yu, and Y. Yan, "Incorporation of n–zno/cds/graphene oxide composite photocatalyst for enhanced photocatalytic activity under visible light," *Journal of Alloys and Compounds*, vol. 670, pp. 198–209, 2016.

[87] P. V. Kamat, "Graphene-based nanoarchitectures. anchoring semiconductor and metal nanoparticles on a two-dimensional carbon support," *The Journal of Physical Chemistry Letters*, vol. 1, no. 2, pp. 520–527, 2009.

[88] H. A. Becerril, J. Mao, Z. Liu, R. M. Stoltenberg, Z. Bao, and Y. Chen, "Evaluation of solution-processed reduced graphene oxide films as transparent conductors," *ACS nano*, vol. 2, no. 3, pp. 463–470, 2008.

[89] N. A. Kotov, I. Dékány, and J. H. Fendler, "Ultrathin graphite oxide–polyelectrolyte composites prepared by self-assembly: Transition between conductive and non-conductive states," *Advanced Materials*, vol. 8, no. 8, pp. 637–641, 1996.

[90] M. Gondal, Z. Yamani, Q. Drmosh, and A. Rashid, "Synthesis of nanostructured zno and zno2 by laser ablation process using third harmonic of nd: Yag laser," *International Journal of Nanoparticles*, vol. 2, no. 1-6, pp. 119–128, 2009.

[91] Y. Xu and M. A. Schoonen, "The absolute energy positions of conduction and valence bands of selected semiconducting minerals," *American Mineralogist*, vol. 85, no. 3-4, pp. 543–556, 2000.

[92] D. Pan, S. Wang, B. Zhao, M. Wu, H. Zhang, Y. Wang, and Z. Jiao, "Li storage properties of disordered graphene nanosheets," *Chemistry of Materials*, vol. 21, no. 14, pp. 3136–3142, 2009.

[93] S. Das, K. Bhattacharjee, S. Maitra, and G. Das, "Effect of oxygen partial pressure on the photoluminescence properties of sol–gel synthesized nanostructured zno thin films," *Thin Solid Films*, vol. 550, pp. 65–70, 2014.

[94] R. S. Dey and C. R. Raj, "A hybrid functional nanoscaffold based on reduced graphene oxide–zno for the development of an amperometric biosensing platform," *RSC Advances*, vol. 3, no. 48, pp. 25 858–25 864, 2013.

[95] M. Kavitha, P. Gopinath, and H. John, "Reduced graphene oxide–zno self-assembled films: tailoring the visible light photoconductivity by the intrinsic defect states in zno," *Physical Chemistry Chemical Physics*, vol. 17, no. 22, pp. 14 647–14 655, 2015.

[96] J. H. Nobbs, "Kubelkamunk theory and the prediction of reflectance," *Coloration Technology*, vol. 15, no. 1, pp. 66–75, 1985.

[97] J. Tauc, "Optical properties and electronic structure of amorphous ge and si," *Materials Research Bulletin*, vol. 3, no. 1, pp. 37–46, 1968.

Vitae

- Name: Redhwan Abdo Qasem Moqbel
- Nationality: Yemen
- Date of Birth: 05/05/1986
- Email: *Redhwanalsamee@yahoo.com*
- Permenant Address: Taiz-Yemen
- Publications:

[1] R. A. Moqbel, M. A. Gondal, T. F. Qahtan, and M. A. Dastageer, Synthesis of cadmium sulfidereduced graphene oxide nanocomposites by pulsed laser ablation in liquid for the enhanced photocatalytic reactions in the visible light, Int. J. Energy Res., vol. 42, no. 4, pp. 14871495, 2018.

[2] R. A. Moqbel, M. A. Gondal, T. F. Qahtan, and M. A. Dastageer, Pulsed laser synthesis in liquid of efficient visible-light-active ZnO/rGO nanocomposites for improved photo-catalytic activity, Mater. Res. Express, vol. 5, no. 3, p. 35050, 2018.

[3] Q. A. Drmosh, Z. H. Yamani, A. H. Y. Hendi, A. Gondal, and R. A. Moqbel, Topic: Chemical sensors A low Temperature H 2 Gas Sensor Based on Pt-loaded Reduced Graphene Oxide / ZnO Nanocomposites, 17th Int. Meet. Chem. Sensors - IMCS 2018, pp. 23, 2018.

[4] R. A. Moqbel, M. A. Gondal, T. F. Qahtan, and A. Lais, Photocatalytic application of CdS nanoparticles and CdS/RGO hybrid composite synthesized by pulsed laser ablation method, AIP Conf. Proc., vol. 1976, pp. 15, 2018.

[5] Q.A.Drmosh, Z.H.Yamani, R.A. Moqbel, M. A. Gondal, A novel approach to fabricate rGO/ZnO/Pt system as ultra-sensitive H2 gas sensor at low operating temperature (Accepted)

[6] R.A. Moqbel, M. A. Gondal, T. F. Qahtan, M. A. Dastageer, 2017, Fabrication of ZnO/ZnO2 nanocomposites by Pulsed Laser Ablation in Liquid and Their Applications under visible light. (In progress)